Title

Characterization of initial key steps of IL-17 receptor B oncogenic signaling for targeted therapy of pancreatic cancer

Journal

Science Translational Medicine, 13(583)

ISSN

1946-6234

Authors

Wu, Heng-Hsiung

Tsai, Lung-Hung

Huang, Chun-Kai

et al.

Publication Date

2021-03-03

DOI

10.1126/scitranslmed.abc2823

CORRECTED 7 DECEMBER 2022; SEE ERRATUM

CANCER

Characterization of initial key steps of IL-17 receptor B oncogenic signaling for targeted therapy of pancreatic cancer

Heng-Hsiung Wu[1,2], Lung-Hung Tsai[1], Chun-Kai Huang[3], Pang-Hung Hsu[4,5], Mei-Yu Chen[1], Yi-Ing Chen[3], Chun-Mei Hu[3], Chia-Ning Shen[3], Chen-Chen Lee[1,6], Ming-Chu Chang[7], Yu-Ting Chang[7], Yu-Wen Tien[8], Yung-Ming Jeng[9], Eva Y.-H.P. Lee[3,10], Wen-Hwa Lee[1,3,10]*

The members of the interleukin-17 (IL-17) cytokine family and their receptors were identified decades ago. Unlike IL-17 receptor A (IL-17RA), which heterodimerizes with IL-17RB, IL-17RC, and IL-17RD and mediates proinflammatory gene expression, IL-17RB plays a distinct role in promoting tumor growth and metastasis upon stimulation with IL-17B. However, the molecular basis by which IL-17RB promotes oncogenesis is unknown. Here, we report that IL-17RB forms a homodimer and recruits mixed-lineage kinase 4 (MLK4), a dual kinase, to phosphorylate it at tyrosine-447 upon treatment with IL-17B in vitro. Higher amounts of phosphorylated IL-17RB in tumor specimens obtained from patients with pancreatic cancer correlated with worse prognosis. Phosphorylated IL-17RB recruits the ubiquitin ligase tripartite motif containing 56 to add lysine-63–linked ubiquitin chains to lysine-470 of IL-17RB, which further assembles NF-κB activator 1 (ACT1) and other factors to propagate downstream oncogenic signaling. Consequentially, IL-17RB mutants with substitution at either tyrosine-447 or lysine-470 lose their oncogenic activity. Treatment with a peptide consisting of amino acids 403 to 416 of IL-17RB blocks MLK4 binding, tyrosine-477 phosphorylation, and lysine-470 ubiquitination in vivo, thereby inhibiting tumorigenesis and metastasis and prolonging the life span of mice bearing pancreatic tumors. These results establish a clear pathway of how proximal signaling of IL-17RB occurs and provides insight into how this pathway provides a therapeutic target for pancreatic cancer.

INTRODUCTION

The interleukin-17 (IL-17) family consists of at least six ligands (A to F) with 20 to 50% sequence homology and five cognate receptors (RA to RE) (*1*). IL-17A, IL-17C, IL-17E, and IL-17F mainly play roles in mediating inflammation in autoimmune, allergic, and chronic inflammatory diseases, whereas the roles of IL-17B and IL-17D are less clear in terms of inflammatory function (*1*). The IL-17 receptors are single-pass transmembrane proteins with conserved structural features (*2*). Specifically, they contain two extracellular fibronectin III–like domains and a cytoplasmic SEFIR (similar expression to fibroblast growth factor genes and IL-17R) domain, which has a role in triggering downstream signaling (*3*). IL-17RA mediates signaling through heterodimerization with IL-17RC for IL-17A and IL-17F, with IL-17RB for IL-17E, with IL-17RE for IL-17C (*4*), and with IL-17RD for IL-17A (*5*). However, whether IL-17B binds to IL-17RB homodimers or heterodimers (*6*, *7*) remains unclear.

Despite the IL-17 receptor family similarity, each receptor has its own distinct structural characteristics. Through detailed genetic analysis, IL-17RA contains about 100 additional residues beyond the SEFIR domain, termed the SEFIR extension domain, which is also required for signaling (*8*, *9*). On the basis of x-ray crystallographic studies, both domains form a single composite structural motif (*10*). Moreover, the cytoplasmic tail of IL-17RA contains a distinct domain, termed the C/EBP-b (CCAAT/enhancer binding protein b) activation domain (CBAD), which binds to tumor necrosis factor receptor–associated factor 3 (TRAF3) and the ubiquitin-editing enzyme A20 (*11*–*13*). However, unlike IL-17RA, the SEFIR region of IL-17RB exhibits a very different three-dimensional topology (*10*, *14*), and its C terminus lacks the CBAD domain, suggesting that IL-17RB may operate in a distinct manner from IL-17RA.

Cancer cells are known to exploit signaling pathways responsible for cell proliferation, division, differentiation, and migration to gain a growth advantage. Proinflammatory cytokines are involved in tumor progression through modulation of the inflammatory tumor microenvironment (*15*). Nevertheless, it is rarely found that alterations of proinflammatory cytokine signal pathway inside tumor cells drive cancer progression. However, overexpression of IL-17RB in pancreatic cancer (*7*), breast cancer (*6*, *16*, *17*), and other neoplasms correlates with their malignancy. Depletion of IL-17RB or treatment with neutralizing antibodies against IL-17RB abolished tumor growth and metastasis (*7*), suggesting the importance of this receptor in these cancers. This potential oncogenic function of IL-17RB is similar to well-recognized receptor tyrosine kinases (RTKs), which play a critical role in oncogenic processes in many cancers. RTKs are generally activated by receptor-specific ligands by binding to extracellular regions of RTKs, and the receptor is activated by ligand-induced receptor dimerization or oligomerization (*18*). For most RTKs, this conformational change allows the kinase domain to assume an active conformation for autophosphorylation of RTKs and engages downstream mediators that propagate critical cellular

[1]Drug Development Center, China Medical University, Taichung 40402, Taiwan. [2]Graduate Institute of Biomedical Sciences, China Medical University, Taichung 40402, Taiwan. [3]Genomics Research Center, Academia Sinica, Taipei 11529, Taiwan. [4]Institute of Biochemistry and Molecular Biology, National Yang Ming University, Taipei 11221, Taiwan. [5]Department of Bioscience and Biotechnology, National Taiwan Ocean University, Keelung 20224, Taiwan. [6]Department of Microbiology and Immunology, China Medical University, Taichung 40402, Taiwan. [7]Department of Internal Medicine, National Taiwan University Hospital, Taipei 10041, Taiwan. [8]Department of Surgery, National Taiwan University Hospital, Taipei 10041, Taiwan. [9]Department of Pathology, National Taiwan University Hospital, Taipei 10041, Taiwan. [10]Department of Biological Chemistry, University of California, Irvine, CA 92697, USA.
*Corresponding author. Email: whlee@uci.edu

signaling pathways. However, IL-17RB lacks a defined kinase domain and is not an RTK. The mechanism by which IL-17RB responds to its ligand and transmits the signal to downstream mediators for its oncogenic function needs to be determined.

Here, we elucidate the signaling mechanism downstream of IL-17RB. The importance of this signaling mechanism in cancer was further demonstrated by blocking the activation of IL-17RB in vivo, thereby reducing tumorigenesis and metastasis and prolonging the life span of pancreatic tumor–bearing mice.

RESULTS

Phosphorylation of tyrosine-447 is critical for IL-17B–induced signaling by IL-17RB

To explore how IL-17B activates IL-17RB signaling, we used a two-pronged approach by identifying posttranscriptional modification residues of IL-17RB and searching for its interacting enzymes through proteomic analysis. Because the earliest response for most cell surface receptors is phosphorylation upon ligand binding, we first tested whether IL-17RB is phosphorylated at tyrosine (Y), serine (S), or threonine (T) residues upon IL-17B stimulation. Increasing phosphorylation on tyrosine, but not on serine or threonine, of IL-17RB was observed within 5 min of IL-17B addition to CFPAC1 pancreatic tumor cells (Fig. 1A), suggesting that tyrosine phosphorylation of IL-17RB is important for signaling.

To determine which tyrosine residue was phosphorylated, we individually mutated each of the six tyrosine residues in the intracellular domain (ICD) to phenylalanine (F) (Fig. 1B). We ectopically expressed wild type or one of the six mutants in IL-17RB–knockout pancreatic cancer cells. Deletion of IL-17RB in CFPAC1 or BxPC3 pancreatic tumor cells by CRISPR-Cas9 resulted in abrogated cytokine signaling, colony formation, and cell invasion in vitro, suggesting that IL-17RB is required for these functions (fig. S1). When we expressed mutant IL-17RB in IL-17RB–knockout BxPC3 cells, we found that the Y447F mutant had abrogated tyrosine phosphorylation induced by IL-17B (Fig. 1C). A cross-species analysis revealed that Y447 is highly conserved in mammals (fig. S2A). Therefore, we generated a rabbit anti–IL-17RB (P-Y447) antibody, recognizing Y447 phosphorylation (Fig. 1D), and demonstrated that Y447 phosphorylation of IL-17RB was up-regulated by IL-17B in a dose-dependent manner (Fig. 1E). Consequently, we evaluated these cells for their downstream signaling, including extracellular signal-regulated kinase 1/2 (ERK1/2) phosphorylation, cytokine gene expression, and oncogenic behavior, and found that only the cells expressing Y447F exhibited a reduction of IL-17B–induced ERK1/2 phosphorylation (Fig. 1F and fig. S2B), cytokine gene expression [$P = 0.0022$ for CCL20, $P = 0.0043$ for CXCL1, and $P = 0.0022$ for TFF1 (Fig. 1G) and $P = 0.0022$ for all the three genes (fig. S2C)], and colony formation compared to the wild-type control [$P = 0.0022$ (Fig. 1H) and $P = 0.0022$ (fig. S2D)]. These results suggested that phosphorylation of Y447 is critical for IL-17B/IL-17RB signal transduction in pancreatic tumor cells.

Abundance of phospho–IL-17RB correlates with poorer prognosis in patients diagnosed with pancreatic tumors

To determine the clinical importance of IL-17RB Y447 phosphorylation, we first determined the specificity of a phospho–IL-17RB (P-Y447) antibody by immunohistochemistry (IHC) using a xenograft BxPC3 tumor samples. The IHC signal was abolished by preabsorbance of the antibody with P-Y447 peptide (CHKYVVV{pY}FREIDT), but not Y447 peptide (CHKYVVVYFREIDT), suggesting specificity for P-Y447 (Fig. 2A). P-Y447 IHC signal was detected on cell membranes (fig. S3) and associated with the expression of IL-17RB assessed by a monoclonal antibody against IL-17RB ($P < 0.001$; Fig. 2B and fig. S3A). Phosphorylation of IL-17RB correlated with worse prognosis in the overall survival of patients with pancreatic cancer ($P = 0.019$; Fig. 2C). Univariate ($P = 0.007$) and multivariate ($P = 0.006$) analyses revealed that high amounts of P-Y447 alone was associated with poorer outcomes (Fig. 2D and table S1). Moreover, tumor specimens with high Y447 phosphorylation were poorly differentiated (table S2) and had a higher potential to form tumors in mouse xenograft models ($P = 0.001$; Fig. 2E). Among the 44 resected pancreatic tumors used as patient-derived xenografts (Fig. 2E), the presence of high IL-17RB P-Y447 correlated with the worse postoperative progression indicated by recurrence or metastasis ($P = 0.008$; Fig. 2F). Furthermore, larger proportions of tumor specimens with high P-Y447 was obtained from liver metastases (70.6%, 12 of 17) than from primary tumors (32.2%, 28 of 87) ($P = 0.005$ by chi-square test; fig. S3B). Together, these results suggest that phosphorylation of IL-17RB at Y447 is associated with clinically aggressive pancreatic tumors.

Mixed-lineage kinase 4 associates with IL-17RB and is required for signaling downstream of IL-17B stimulation

We next performed coimmunoprecipitation (co-IP) followed by tandem mass spectrometry (MS) analysis to identify proteins associated with IL-17RB upon IL-17B stimuli relative to control bovine serum albumin treatment (fig. S4A). As shown in table S3, 126 proteins coimmunoprecipitated with IL-17RB after IL-17B stimulation. The top three proteins that coimmunoprecipitated and have kinase activity include adaptor-related protein complex 2–associated protein kinase 1 (AAK1), homeodomain-interacting protein kinase 1 (HIPK1), and mixed-lineage kinase 4 (MLK4; also known as KIAA1804 and MAP3K21) (fig. S4B). Upon IL-17B treatment, these three proteins interacted with IL-17RB in a dose-dependent manner (Fig. 3A). Only knockdown of MLK4 (Fig. 3B), but not AAK1 (fig. S4C), HIPK1 (fig. S4D), or spleen tyrosine kinase (Syk) (fig. S4E), attenuated ERK1/2 phosphorylation induced by IL-17B. Moreover, on the basis of reciprocal co-IP assay (Fig. 3C) and proximity ligation assay (PLA) ($P < 0.0001$; Fig. 3D), IL-17RB and MLK4 directly interacted upon IL-17B addition. Because MLK4 is a poorly characterized kinase (*19*), we tested whether MLK4 is involved in oncogenic signaling by depleting MLK4 expression in both pancreatic (CFPAC1, AsPC1, and BxPC3) and breast (MB361 and MB468) cancer cell lines. IL-17B–induced ERK1/2 phosphorylation (fig. S5A), cytokine gene expression (Fig. 3E and fig. S5B), colony formation (Fig. 3F and fig. S5C), and cell invasion activity (fig. S5D) were all abrogated in MLK4-knockdown cancer cells. These data suggest that MLK4 is essential for IL-17RB signal transduction in tumor cells.

IL-17RB homodimerization is required for recruiting MLK4

It has been previously reported that IL-17RA heterodimerizes upon specific ligand binding to initiate intracellular signaling (*20*, *21*). Although IL-17RB forms heterodimers with IL-17RA for IL-17E binding, it is unclear whether IL-17RB binds to another receptor chain for IL-17B binding. No other member of the IL-17 receptor family was found to interact with IL-17RB after IL-17B stimulation, suggesting that IL-17RB may homodimerize after IL-17B binding

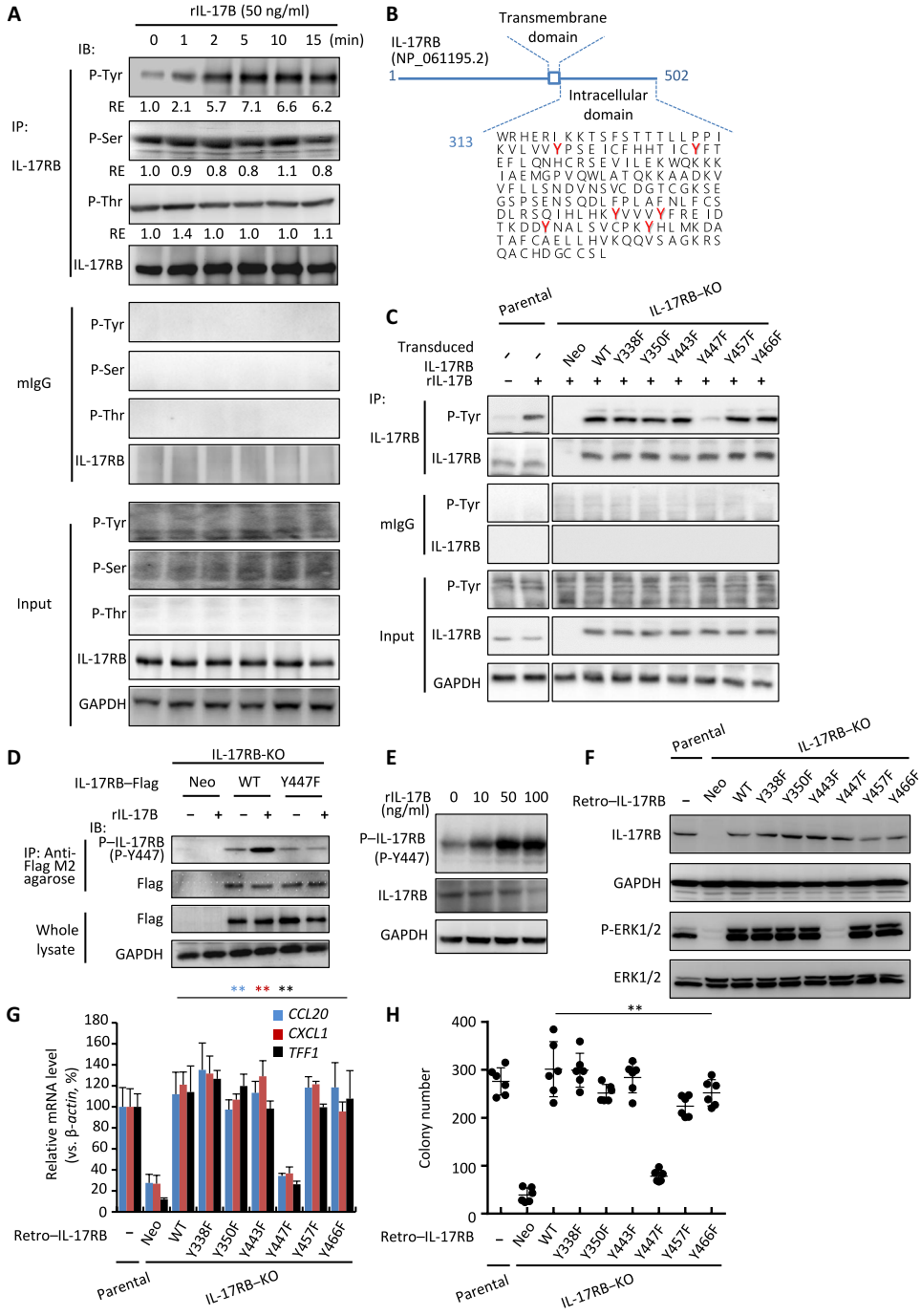

Fig. 1. Tyrosine-447 in the intracellular domain of IL-17RB is critical for IL-17RB signaling. (**A**) Immunoblots (IB) of phosphorylation at tyrosine, serine, and threonine residues of IL-17RB immunoprecipitated (IP) by anti–IL-17RB antibody (D9) from CFPAC1 cells treated with rIL-17B. $N = 2$. (**B**) Sequence of the IL-17RB intracellular domain with the six tyrosine residues highlighted in red. (**C**) Immunoblotting analysis of IL-17RB–knockout (KO) BxPC3 cells expressing the wild type (WT) and six tyrosine (Y)–to–phenylalanine (F) mutants of IL-17RB. IL-17RB–knockout BxPC3 cells were treated with recombinant IL-17B (rIL-17B), and the cell lysates were immunoprecipitated with anti-IL-17RB or control mouse immunoglobulin G (mIgG), followed by immunoblotting with the indicated antibodies or directly immunoblotted with the indicated antibodies as the input control. $N = 2$. (**D**) The P-Y447 antibody recognizes WT, but not Y447F, IL-17RB after IL-17B treatment. IL-17RB–knockout BxPC3 cells expressing Flag-tagged WT and Y447F-mutant IL-17RB were treated with rIL-17B, and the cell lysates were immunoprecipitated by anti-Flag–conjugated beads. The blot was probed by P-Y447–specific antibody or directly immunoblotted with the antibodies indicated as the input control. $N = 2$. (**E**) IL-17B results in phosphorylation of IL-17RB Y447 in a dose-dependent manner. BxPC3 cells were treated with the indicated amounts of rIL-17B, and the cell lysates were immunoblotted with the indicated antibodies. $N = 3$. (**F**) Immunoblotting analysis of ERK1/2 phosphorylation in CFPAC1 cells expressing WT or mutant IL-17RB with the indicated antibodies. $N = 2$. (**G**) Relative mRNA expression of *CCL20*, *CXCL1*, and *TFF1* in WT or mutant IL-17RB–expressing CFPAC1 cells stimulated with IL-17B was measured by RT-qPCR ($n = 6$). $N = 2$. (**H**) WT and mutant IL-17RB–expressing cells were evaluated by a soft agar colony formation (SACF) assay ($n = 6$). ($N = 3$). Data in (G) and (H) are means ± SD. $^{**}P < 0.001$ by one-way analysis of variance (ANOVA).

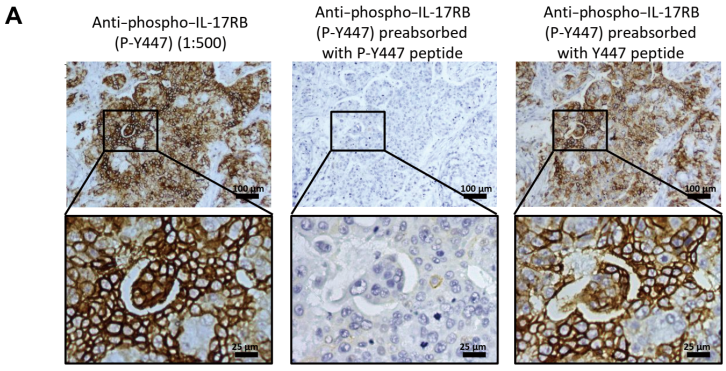

B

IHC staining	Total N	Phospho–IL-17RB (P-Y447) Low, n (%)	High, n (%)	P value
	87	59 (68)	28 (32)	
IL-17RB (A81)				
Low	51	51 (100)	0 (0)	P < 0.001
High	36	8 (22)	28 (78)	

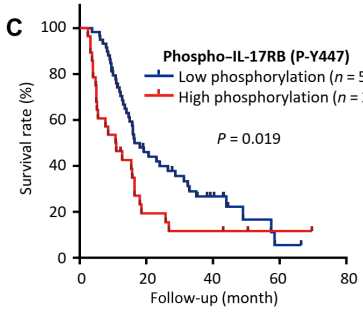

D

Variants	Patient no. (%)	Hazard ratio (95% CI)	P value
Univariate:			
Phospho–IL-17RB: High (vs. low)	28 (32)	1.963 (1.209–3.190)	0.007
Multivariate§:			
Phospho–IL-17RB: High (vs. low)	28 (32)	2.314 (1.276–4.196)	0.006

§ Adjusted with clinical and pathological parameters of age, gender, *T* value, *N* value, AJCC stage, margin involvement, lymphovascular invasion, and perineuronal invasion (table S1).

E

IHC staining	Total N	Patient-derived xenograft None n (%)	Tumor formation n (%)	P value
	44	26 (59)	18 (41)	
Phospho–IL-17RB (P-Y447)				
Low	26	21 (81)	5 (19)	0.001
High	18	5 (28)	13 (72)	

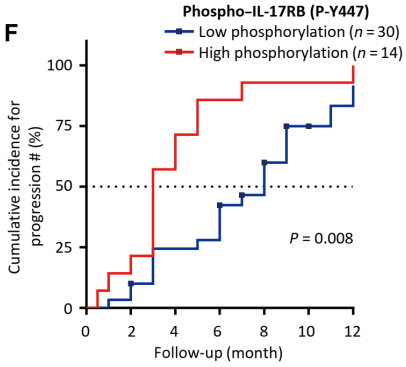

Fig. 2. Phosphorylation of IL-17RB Y447 correlates with worse prognosis for patients with pancreatic cancer. (**A**) Representative IHC images of three serial sections of BxPC3 xenografts isolated from NOD-SCID mice and stained with anti–P-Y477 or peptide-preabsorbed antisera to verify antibody specificity. (**B**) Correlation between IL-17RB expression and IL-17RB phosphorylation in 87 patients with pancreatic cancer. *P* values were determined by a chi-square test. (**C**) Overall survival of 87 patients with pancreatic cancer with different low or high phosphorylation of Y447 expression was plotted with the Kaplan-Meier method. *P* values were determined by a log-rank test. (**D**) Univariate and multivariate Cox regression analysis of the influence of P-Y447 on the overall survival of 87 patients with pancreatic cancer after surgical therapy. *P* values were determined by chi-square test. AJCC, American Joint Committee on Cancer. (**E**) P-Y447 in cancer cells correlates with tumor formation in patient-derived xenografts in 44 pancreatic cancer specimens. *P* values were determined by chi-square test. (**F**) The proportion of postoperative progression within 1 year of 44 patients with pancreatic cancer with high or low phosphorylation of Y447 was plotted over time. The dotted line indicates the median time of cancer progression. Progression was defined by postoperative recurrence or metastasis. *P* value was determined by a log-rank test.

(table S3). To test this possibility, we cotransfected hemagglutinin (HA)– and Flag-tagged IL-17RB (IL-17RB–HA and IL-17RB–Flag, respectively) into IL-17RB–knockout cells for co-IP experiments after IL-17B addition. Consistent with increased MLK4 binding and ERK1/2 phosphorylation, IL-17RB homodimerization was induced by IL-17B in a time-dependent manner (Fig. 4A). To confirm this finding, we expressed IL-17RB wild type or mutant (IL-17RB^{FNmut}–Flag), in which the putative dimerization domain (fibronectin-like domain 2) (*22*) was truncated (fig. S6A), in BxPC3 cells (fig. S6, B and C) for co-IP experiments after IL-17B addition. Unlike wild-type IL-17RB, IL-17RB^{FNmut} failed to form homodimers after stimulation (Fig. 4B). Similar results were obtained via a PLA. PLA signal, suggesting homodimerization, was observed in cells ectopically expressing wild-type IL-17RB but not IL-17RB^{FNmut} upon IL-17B stimulation ($P < 0.0001$; Fig. 4C and fig. S6D). Further, PLA signal was observed between endogenous IL-17RB molecules on the surface of CFPAC1 cells after IL-17B stimulation ($P < 0.0001$; Fig. 4D). Moreover, abrogation of IL-17RB dimerization not only inhibited MLK4 binding (Fig. 4E) but also abolished IL-17B–induced phosphorylation of IL-17RB Y447 and ERK1/2 (Fig. 4F). Consistently, CFPAC1 or BxPC3 cells expressing IL-17RB^{FNmut} reduced cytokine mRNA expression after IL-17B stimulation relative to IL-17RB wild-type control cells ($P = 0.0079$ for CCL20, $P = 0.0022$ for CXCL1, and $P = 0.0022$ for TFF1; Fig. 4G and fig. S6E) and colony formation ability ($P = 0.0022$; Fig. 4H and fig. S6F). These results suggest that IL-17B triggers homodimerization of IL-17RB for MLK4 binding and downstream signal transduction.

IL-17RB has two different ligands: IL-17E and IL-17B (*23*, *24*). Unlike IL-17B, IL-17E binds to IL-17RA/IL-17RB heterodimer to activate T helper cell 2 (T_H2) immune responses (*24*–*26*). To validate the specificity of IL-17RB dimerization in response to IL-17B, we performed co-IP experiments using IL-17RB–knockout cells ectopically expressing IL-17RB–HA and IL-17RB–Flag and His-tagged IL-17RA (Fig. 4I). We found that IL-17B specifically induced IL-17RB homodimerization (Fig. 4, C, E and I) but IL-17B stimulation did not induce heterodimerization of IL-17RA and IL-17RB as compared to IL-17E stimulation (Fig. 4I). Consequently, IL-17B, but not IL-17E, induced MLK4 binding to IL-17RB (Fig. 4, E and I) and phosphorylation of IL-17RB (fig. S6G).

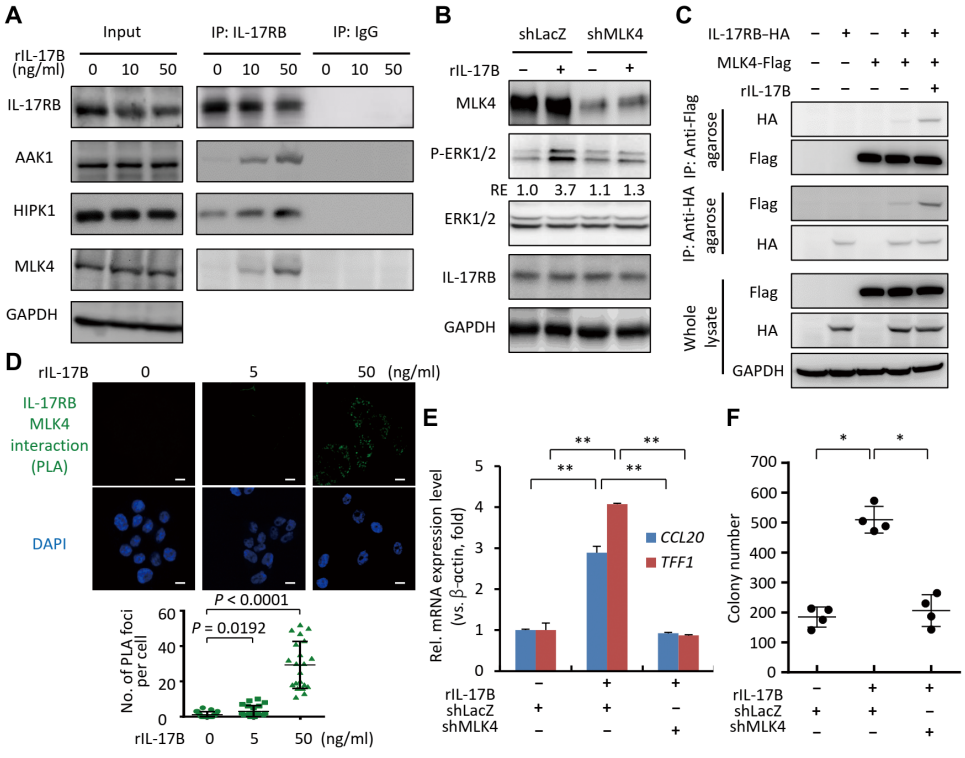

Fig. 3. MLK4 is required for IL-17B signaling through IL-17RB in pancreatic cancer cells. (**A**) Immunoblotting analysis of IL-17RB binding to AAK1, HIPK1, and MLK4. CFPAC1 cells were treated with the indicated concentrations of rIL-17B, and the cell lysates were coimmunoprecipitated with anti–IL-17RB and blotted with the indicated antibodies or directly immunoblotted with the indicated antibodies as the input controls. $N = 3$. (**B**) Immunoblotting analysis of MLK4 depletion and ERK1/2 phosphorylation. CFPAC1 cells were depleted by the corresponding lenti-shRNAs of shMLK4 or shLacZ as a control, and the cell lysates were directly immunoblotted with the indicated antibodies. RE indicates relative amount. $N = 2$. (C) Coimmunoprecipitation of MLK4 and IL-17RB. 293T cells cotransfected with IL-17RB–HA and Flag-MLK4 were treated with rIL-17B, and the cell lysates were reciprocally coimmunoprecipitated with anti-Flag– and anti-HA–conjugated beads and followed by immunoblotting analysis with the indicated antibodies. $N = 3$. (D) Representative image micrographs (top) and quantification (bottom) of in situ proximity ligation assay (PLA). The interaction between IL-17RB and MLK4 was analyzed in BxPC3 cells using anti–IL-17RB and anti-MLK4 antibodies after rIL-17B treatment. Scale bars, 5 μm. Green dots, representing interactions, in the cells were scored ($n = 20$). Data were means ± SD. P value was determined by Mann-Whitney test. $N = 3$. (**E** and **F**) MLK4-knockdown CFPAC1 cells were evaluated for cytokine mRNA expression by RT-qPCR ($n = 6$) (E) or for SACF assay ($n = 4$) (H). $N = 3$. Data in (E) and (F) were means ± SD. *$P < 0.05$ and **$P < 0.01$ by Mann-Whitney test.

Moreover, ectopically expressing IL-17RA not only suppressed IL-17B–induced IL-17RB homodimerization and phosphorylation but also facilitated IL-17E–mediated inhibition of IL-17RB dimerization and phosphorylation (fig. S7). Furthermore, homodimerization of IL-17RB induced by IL-17B was not affected by depletion of MLK4 or mutation of Y447 (fig. S8), indicating that the dimerization of IL-17RB was a prerequisite for downstream signaling events. Together, these results suggest that IL-17B signaling cascade via IL-17RB is distinct from the other IL-17 receptor family members.

MLK4 specifically phosphorylates IL-17RB at Y447 through binding to the flexible loop of IL-17RB

MLK4 belongs to the MLK family, whose members have both serine/threonine and tyrosine kinase domains (*19*, *27*). Although MLKs are known to have functional serine/threonine kinase activity (*28*, *29*), their tyrosine kinase activity is rarely displayed. Because both phosphorylation of IL-17RB (Fig. 1 and fig. S6G) and MLK4 binding to IL-17RB were observed (Fig. 4, E and I) upon IL-17B, but not IL-17E, stimulation, it is likely that IL-17RB is a substrate of MLK4. We found that either knockdown (left) or knockout (right) of MLK4 nearly completely abolished IL-17RB phosphorylation at Y447 in both pancreatic and breast cancer cells (Fig. 5A and fig. S9A). These results suggest that no other cellular kinase could substitute MLK4 enzymatic activity for tyrosine phosphorylation of IL-17RB.

To further assess the biological impact of MLK4 in IL-17B/IL-17RB signaling in an in vitro culture system, we performed rescue experiments by ectopically expressing wild-type or known MLK4 mutants (SH3 mutant, Δ100-108; kinase-dead mutant, E314K and Y330H) (*30*) in MLK4-knockout cells. Ectopic expression of the wild-type MLK4, but not either mutant, restored IL-17B–induced phosphorylation on IL-17RB Y447 and ERK1/2 (Fig. 5B), as well as downstream gene expression ($P < 0.0001$ for CCL20, CXCL1, and TFF1; Fig. 5C). Furthermore, when we used a pan-MLK inhibitor, CEP-1347, to treat the high IL-17RB–expressing breast and pancreatic cancer cells, we found that the phosphorylation of both ERK1/2 and IL-17RB (fig. S9A), cytokine gene expressions ($P < 0.05$; fig. S9B), invasion ($P = 0.0286$; fig. S9C), and colony formation properties of the cancer cells were abrogated ($P = 0.0286$; fig. S9D). These data further suggest that MLK4-mediated phosphorylation of Y447 of IL-17RB is essential for IL-17B/IL-17RB signaling.

Next, to explore the critical interaction region of IL-17RB essential for the MLK4 binding, we modeled the ICD of human IL-17RB based on the structure of mouse Il-17rb (3vbc) (fig. S10). This revealed that the ICD is composed of five α helices, five β sheets, and a flexible loop (fig. S10A) and that mouse Y444 (homologous to human Y447) is located on the surface of the ICD (fig. S10B). We then constructed eight individual mutants by deleting core residues of the α helix and flexible loop distributed on the surface of the IL-17RB ICD (Fig. 5D). The deleted IL-17RB mutants and Flag-MLK4 were ectopically coexpressed in 293T cells for reciprocal co-IP experiments. The ΔV403 ~ S416 mutant (Del-3) alone abrogated IL-17B–induced binding of IL-17RB and MLK4 (Fig. 5E). To assess the biological activity of Del-3, the low IL-17RB–expressing pancreatic cancer cell line SU.86.86 was transfected to ectopically express Del-3 or wild-type IL-17RB, and the cell lysates were assayed for MLK4 binding and Y447 phosphorylation. Del-3 failed to bind to MLK4 and phosphorylate Y447 (Fig. 5F). Cells expressing Del-3 displayed diminished ERK1/2 phosphorylation (Fig. 5F), *CCL20* and *TFF1* expression ($P = 0.0238$ for CCL20 and $P = 0.0022$ for TFF1; Fig. 5G) as well as reduced invasion ($P = 0.0286$; Fig. 5H),

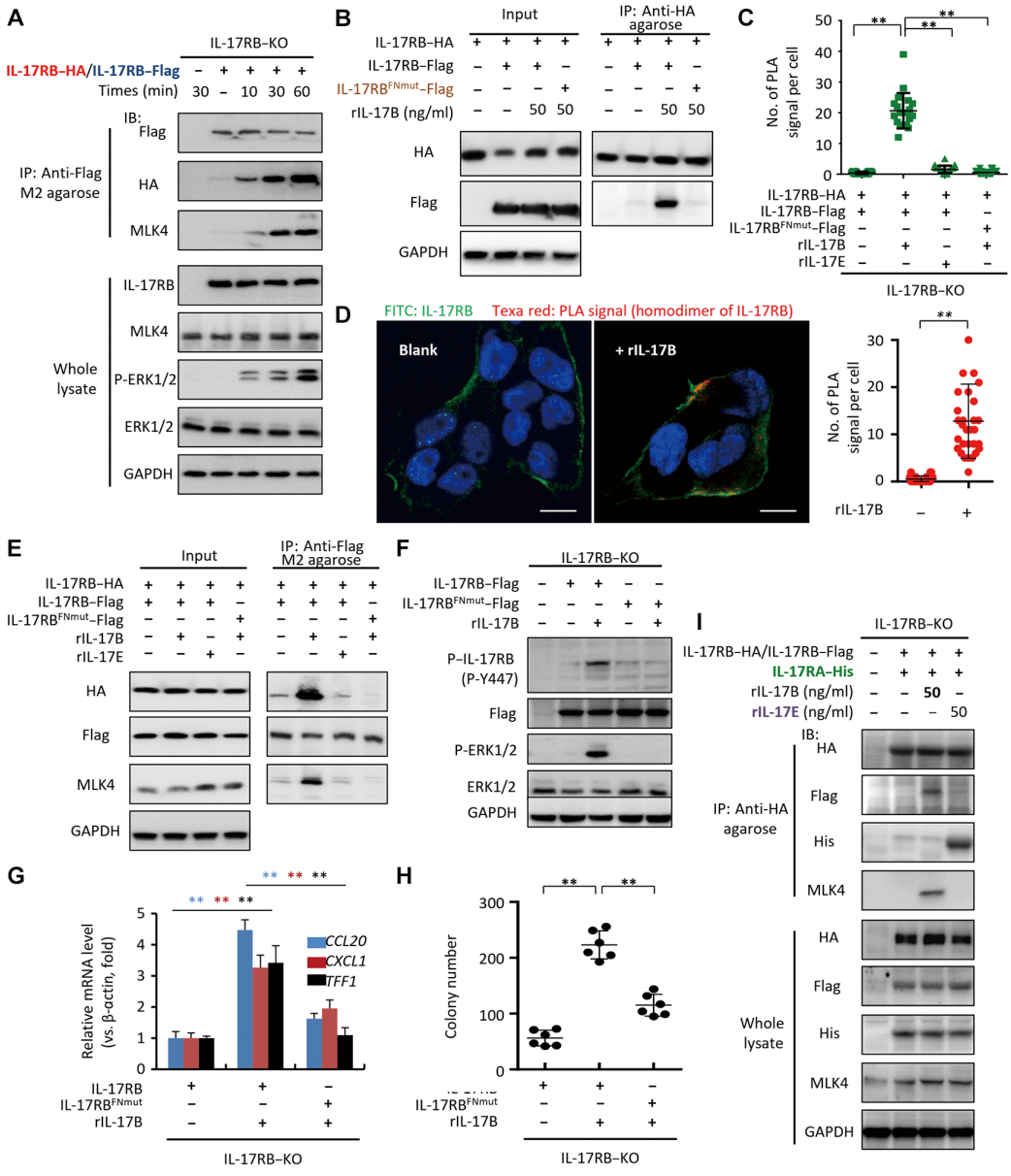

Fig. 4. Homodimerization of IL-17RB recruits MLK4 for downstream signaling. (**A**) Immunoblotting analysis of IL-17RB homodimerization induced by IL-17B. IL-17RB–knockout BxPC3 cells cotransfected with IL-17RB–HA and IL-17RB–Flag were treated with rIL-17B for the indicated time. The cell lysates were immunoprecipitated with anti-Flag–conjugated beads and immunoblotted with the indicated antibodies or directly immunoblotted with the indicated antibodies as the input controls. $N = 2$. (**B**) Immunoblotting analysis of IL-17RB^{FNmut} mutant homodimerization. 293T cells expressing IL-17RB–HA was cotransfected with IL-17RB–Flag or IL-17RB^{FNmut}–Flag and treated with rIL-17B. The cell lysates were immunoprecipitated with anti-HA–conjugated beads and immunoblotted with the indicated antibodies or directly immunoblotted with the indicated antibodies as the input controls. $N = 2$. (**C**) PLA. IL-17RB–knockout BxPC3 expressing IL-17RB–HA–expressing IL-17RB–Flag or IL-17RB^{FNmut}–Flag were treated with IL-17B or IL-17E and subjected for PLA using anti-HA and anti-Flag as probes. The plot shows the numbers of the positive green dots. Data were means ± SD. $^{**}P < 0.01$ by Mann-Whitney test. $N = 2$. (**D**) PLA of the endogenous IL-17RB in response to IL-17B. CFPAC1 cells treated with rIL-17B (50 ng/ml) for 30 min were stained with fluorescein isothiocyanate (FITC)–labeled anti–IL-17RB (D9), after PLA with two mouse secondary antibodies carrying PLA probes (named anti-mouse PLUS and anti-mouse MINUS). Dimerization of IL-17RB upon rIL-17B treatment was revealed by the red dots at the membrane (left). Scale bars, 5 μm. Quantification of the red dots ($n = 25$) was shown in the right panel. *P* value was determined by Mann-Whitney test. (**E**) Immunoblot analysis of IL-17RB^{FNmut} binding to MLK4 upon IL-17B or IL-17E stimulation. The cells, same as in (C), were treated with rIL-17B or rIL-17E (50 ng/ml) for 30 min, and the cell lysates were immunoprecipitated with anti-Flag–conjugated beads and immunoblotted with the indicated antibodies or directly immunoblotted with the indicated antibodies as the input controls. $N = 2$. (**F**) Immunoblot analysis of IL-17RB^{FNmut} in IL-17B–induced IL-17RB Y447 and ERK1/2 phosphorylation. The same cells as (C) were lysed, and the whole cell lysates were directly immunoblotted with the indicated antibodies. $N = 2$. (**G**) Relative expression of *CCL20*, *CXCL1*, and *TFF1* mRNA in IL-17RB–knockout CFPAC1 cells was measured after rIL-17B treatment by RT-qPCR ($n = 6$). (**H**) Indicated cells, same as in (G), were evaluated for colony formation using an SACF assay ($n = 6$). Data in (G) and (H) were means ± SD. $^{**}P < 0.01$ by Mann-Whitney test. $N = 2$. (**I**) Immunoblot analysis of distinct dimerization pattern of IL-17RB upon IL-17B stimulation. IL-17RB–knockout BxPC3 cells were cotransfected with IL-17RB–HA, IL-17RB–Flag, and IL-17RA–His and treated with rIL-17B or rIL-17E, and the cell lysates were immunoprecipitated with anti-HA–conjugated beads after immunoblotted with the indicated antibodies or directly immunoblotted with the indicated antibodies as the input control. $N = 2$.

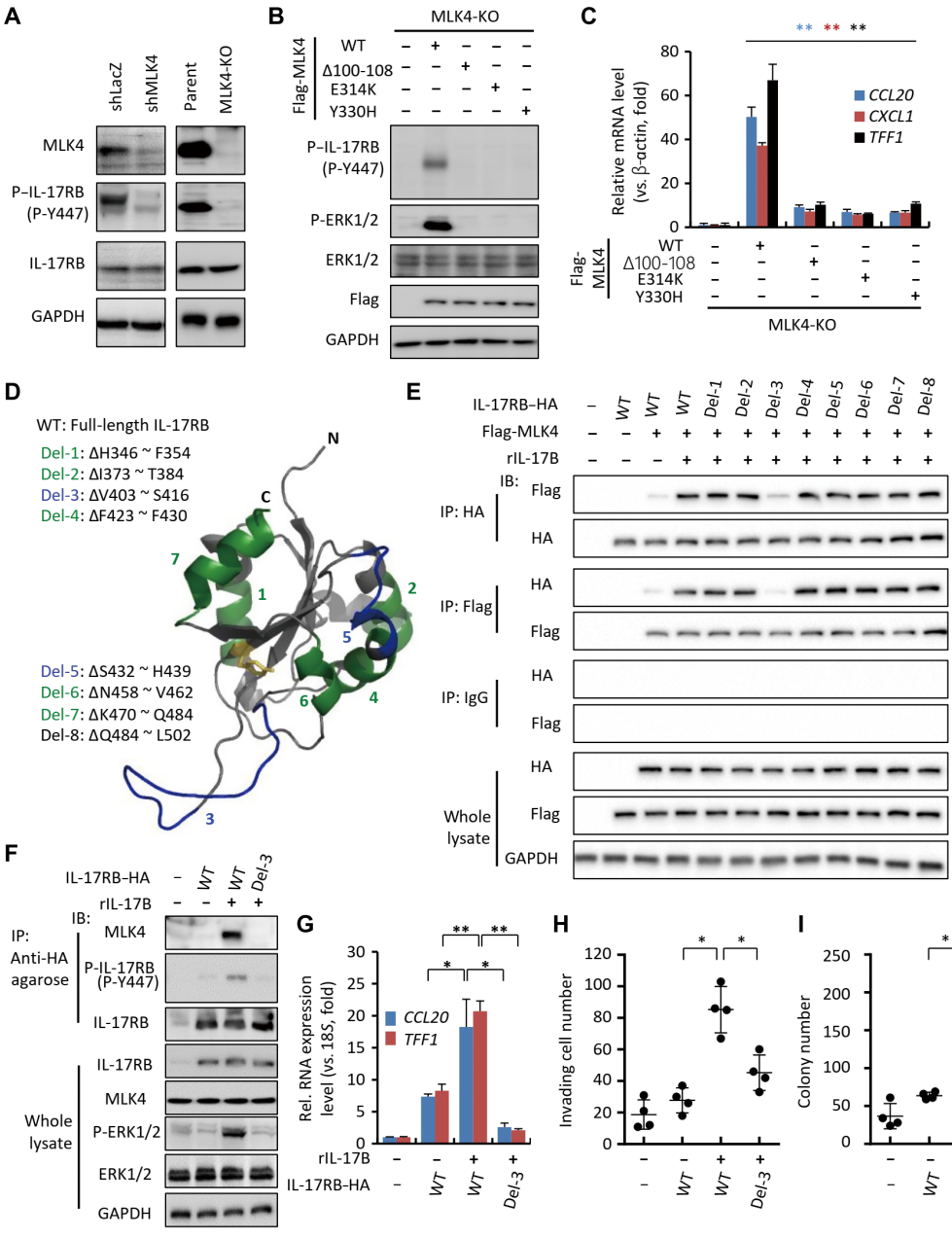

Fig. 5. The flexible loop of IL-17RB is required for MLK4 binding and Y447 phosphorylation of IL-17RB. (**A**) Immunoblotting analysis of MLK4 activity for phosphorylation of Y447 of IL-17RB. WT BxPC3 cells were either treated with shMLK4 or shLacZ and stimulated with rIL-17B, and the cell lysates were immunoblotted with the indicated antibodies (left). WT or MLK4–knockout (KO) BxPC3 cells were stimulated with rIL-17B, and the cell lysates were immunoblotted with the indicated antibodies (right). $N = 3$. (**B**) Flag-tagged WT and kinase mutants (Δ130-138, E314K, and Y330H) of MLK4 were separately expressed in MLK4-knockout BxPC3 cells after rIL-17B treatment. The corresponding cell lysates were directly immunoblotted with the indicated antibodies. $N = 2$. (**C**) *CCL20*, *CXCL1*, and *TFF1* mRNA expression in MLK4-knockout BxPC3 cells was evaluated after rIL-17B treatment by RT-qPCR ($n = 6$). Data were means ± SD. $^{**}P < 0.01$ by Mann-Whitney test. (**D**) A diagram of the human IL-17RB intracellular domain with eight potential subdomains and the list of mutants with the corresponding deleted amino acid sequences are shown. (**E**) 293T cells were cotransfected with Flag-MLK4 and HA-tagged WT or indicated IL-17RB mutant and treated with rIL-17B. The cell lysates were reciprocally coimmunoprecipitated with anti-HA and anti-Flag and blotted with anti-Flag or anti-HA or directly blotted with the indicated antibodies as the input controls. $N = 2$. (**F**) HA-tagged WT or Del-3–mutant IL-17RB were transduced into low IL-17RB–expressing SU.86.86 cells and treated with rIL-17B treatment for 30 min. The cell lysates were subjected to co-IP with anti-HA–conjugated beads, followed by immunoblotting with anti–P-Y447 and anti-MLK4 or directly immunoblotted with the indicated antibodies as the input controls. $N = 2$. (**G**) *CCL20* and *TFF1* mRNA of IL-17RB–knockout BxPC3 cells expressing HA-tagged WT or Del-3 mutant of IL-17RB were measured by RT-qPCR ($n = 6$). (**H** and **I**) WT and Del-3 mutant IL-17RB–expressing cells were further characterized by an invasion assay ($n = 4$) (H) and by a SACF assay ($n = 4$) (I) after treated with rIL-17B (50 ng/ml). Data in (G) to (I) were means ± SD. $^{*}P < 0.05$ and $^{**}P < 0.01$ by Mann-Whitney test. $N = 2$.

and colony formation ($P = 0.0286$; Fig. 5I) capacity as compared to control cells. These results indicate that the flexible loop containing V403 ~ S416 of IL-17RB is critical for MLK4 binding and downstream signaling.

Phosphorylation of IL-17RB at Y447 recruits tripartite motif 56 ubiquitin ligase to add K63-linked ubiquitin onto lysine 470 of IL-17RB

To further evaluate how phosphorylation of IL-17RB at Y447 activates downstream signaling, we performed co-IP and tandem MS analysis to identify the proteins specifically bound to P-Y447 of IL-17RB using IL-17RB–knockout BxPC3 cells that ectopically express wild-type or Y447F-mutant IL-17RB. As listed in table S4, 61 proteins were found to be associated with P-Y447 IL-17RB upon IL-17B stimulation. Among these, the ubiquitin E3 ligase TRIM56 (tripartite motif 56) was of interest because it is known to interact with and mediate K63-linked ubiquitination on stimulator of interferon genes (STING) for the recruitment of TRAF Family Member Associated NF-κB Activator–binding kinase 1 (TBK1) and downstream signaling (*31*). We hypothesized that TRIM56 may regulate IL-17RB in a similar manner. To test this possibility, we performed binding assays in 293T cells (Fig. 6A) or with purified IL-17RB and TRIM56 (fig. S11A) and observed that TRIM56 specifically bound wild type, but not the Y447F-mutant or non–tyrosine-phosphorylated IL-17RB, upon IL-17B stimulation. Moreover, both knockdown and knockout of TRIM56 abrogated IL-17B–induced ERK1/2 phosphorylation (Fig. 6B and fig. S11B), cytokine gene expression (fig. S11C), colony formation (fig. S11D), and invasion (fig. S11E) capacities in both breast and pancreatic cancer cells. These results suggested that TRIM56 plays an essential role in IL-17B/IL-17RB signaling.

To identify the region of IL-17RB that binds to TRIM56, we ectopically coexpressed the eight IL-17RB mutants generated as shown in Fig. 5B and HA-TRIM56 in 293T cells for reciprocal co-IP experiments. The ΔV403 ~ S416 (Del-3), ΔN458 ~ V462 (Del-6), and ΔK470 ~ Q484 (Del-7) mutants failed to bind TRIM56 upon IL-17B stimuli (Fig. 6C). Del-3 failed to bind to TRIM56, as expected, because this region was critical for MLK4 binding and essential for IL-17RB phosphorylation at Y447 (Fig. 5F). Because phosphorylation of Y447 is required for TRIM56 binding, the region spanning N458 to V462, which is near Y447, may be important for IL-17RB to interact with TRIM56. To test this possibility, we ectopically expressed wild type and Del-6 in 293T cells for co-IP experiments and found that Del-6 not only failed to associate with endogenous TRIM56 but also failed to induce ERK1/2 phosphorylation (fig. S11F).

We noticed that IL-17RB ubiquitination induced by IL-17B was composed of K63-linked, but not K48-linked, polyubiquitin (fig. S12A), and depletion of TRIM56 abrogated IL-17B–induced K63-linked ubiquitination of IL-17RB (Fig. 6D). To determine the ubiquitination site of IL-17RB, we substituted three lysine residues on the surface of the IL-17RB ICD (fig. S12B) with arginine to generate individual K333R, K454R, and K470R mutants. These mutants were ectopically expressed in the IL-17RB–knockout cells. In comparison to wild-type IL-17RB, which was polyubiquitinated upon IL-17B binding, the K470R, but not the K333R or K454R mutants, failed to be ubiquitinated (Fig. 6E and fig. S12C), suggesting that the K470 residue was the ubiquitination site of IL-17RB. This finding may partly explain the observation that the deletion of K470 ~ Q484 of IL-17RB compromised TRIM56 binding (Fig. 6C and fig. S11F). Furthermore, purified TRIM56 could ubiquitinate IL-17RB at K470 in vitro (fig. S12D). Together, these results suggest that IL-17RB undergoes K63-linked polyubiquitination at K470 by TRIM56 upon IL-17B induction.

Transmission of IL-17RA signaling includes ligand-induced oligomerization of IL-17RA, recruitment of NF-κB activator 1 (ACT1) through the cytoplasmic SEFIR domain, and activation of the signal axis composed of ACT1, TRAF6, transforming growth factor β–activated kinase 1 (TAK1), and TBK1 (*20*, *32*). It was observed that wild-type, but not K470R-mutant, IL-17RB interacted with ACT1, TRAF6, and TAK1 upon IL-17B induction (Fig. 6F), but knockdown of ACT1 or TRAF6, which has E3 ligase activity, did not affect IL-17B–induced IL-17RB ubiquitination (fig. S12E). Consistently, ectopic expression of the K470R mutant IL-17RB, but not of wild type, in IL-17RB–knockout cells failed to restore cytokine production ($P = 0.0022$ for CCL20 and TFF1; Fig. 6G), colony formation ($P = 0.0286$; Fig. 6H), and cell invasion ($P = 0.0286$; Fig. 6I). These data further indicate that polyubiquitination of IL-17RB at K470 by TRIM56 was critical for IL-17RB signaling.

Homodimerization of IL-17RB induced by IL-17B was not affected by the depletion of TRIM56 or mutation of K470 (fig. S8). Together, these results revealed the pivotal role of Y447 phosphorylation of IL-17RB by MLK4, which led to the recruitment of TRIM56 to polyubiquitinate IL-17RB at K470 in this signaling cascade.

Disruption of the interaction between IL-17RB and MLK4 using a synthetic loop peptide impedes downstream signaling

These mechanistic studies highlighted an opportunity to target and potentially block IL-17RB signaling. To explore this further, we focused on the first step of tyrosine phosphorylation of IL-17RB by MLK4. We considered it likely that a peptide containing the flexible loop of V403 ~ V416 would competitively inhibit MLK4 binding and Y447 phosphorylation. Thus, we synthesized two peptides, a control peptide ($TAT_{48–57}$) and a loop peptide (TAT–$IL\text{-}17RB_{403–416}$) (fig. S13A) and demonstrated that both peptides entered cells by immunofluorescence microscopy (fig. S13B). We then treated cells ectopically expressing both Flag-MLK4 and IL-17RB–HA with these peptides and performed co-IP assays. Treatment with the loop peptide, but not the control peptide, disrupted the interaction between IL-17RB and MLK4 (Fig. 7A) and abolished tyrosine phosphorylation and ubiquitination of IL-17RB (Fig. 7B). Loop peptide treatment also inhibited ERK1/2 phosphorylation induced by IL-17B (Fig. 7B). Moreover, treatment of pancreatic cancer cells expressing IL-17RB with loop peptide diminished cytokine gene expression [$P = 0.0022$ (Fig. 7C) and $P < 0.001$ for CCL20 and TFF1 (fig. S13C)], invasion ($P = 0.0286$; Fig. 7D and fig. S13D), and colony formation ($P = 0.0286$; Fig. 7E and fig. S13E). As expected, unlike anti–IL-17RB antibody, which could inhibit IL-4 and IL-13 expression induced by IL-17E in peripheral blood mononuclear cells (fig. S14, A to C), loop peptide treatment did not interfere IL-4 and IL-13 expression (fig. S14, D and E) nor activate dendritic cells (fig. S14, F and G). These data suggest that the loop peptide had the potential to block IL-17RB signaling specifically induced by IL-17B but not IL-17E.

To test the therapeutic potential of the loop peptide, we used two mouse models of pancreatic cancer. The first model involved spontaneous pancreatic tumors generated in pancreas-specific $Kras^{G12D}$-knockin mice (*LSL-*$Kras^{G12D/+}$*; p53*$^{+/-}$*; Ela-*Cre^{ERT}; EKP mice), in which tumors are induced upon further cerulein treatment (*33*–*35*). Two parallel treatment protocols were used (Fig. 7F). First, we measured

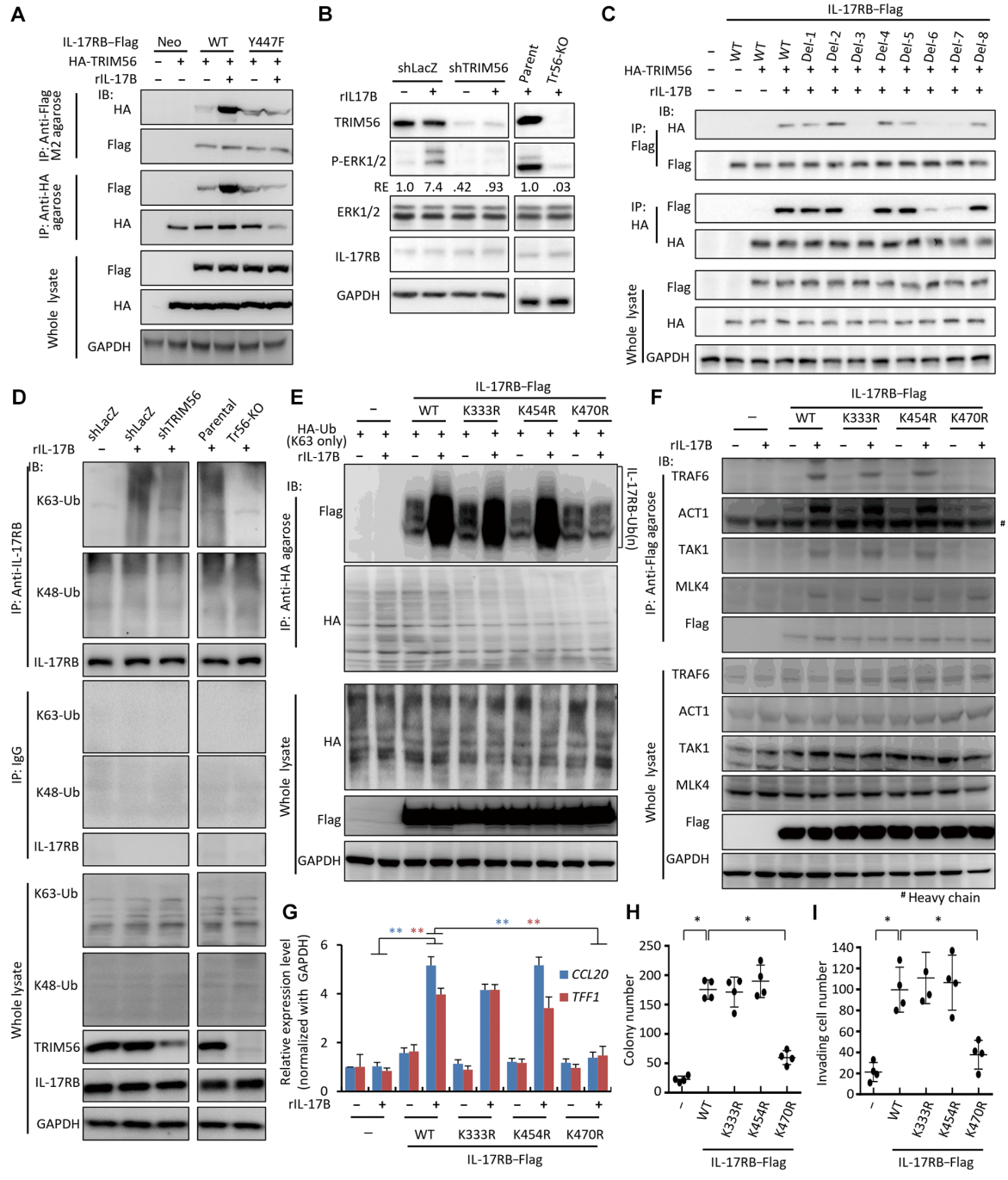

Fig. 6. P-Y447 IL-17RB recruits TRIM56 for K63-linked ubiquitination at K470 of IL-17RB for downstream oncogenic signaling. (**A**) 293T cells expressing both Flag-tagged WT or Y447F-mutant IL-17RB and HA-tagged TRIM56 were treated with rIL-17B, and the cell lysates were coimmunoprecipitated and immunoblotted with the indicated antibodies or directly immunoblotted with the indicated antibodies as the input control. Neo, empty vector. $N = 2$. (**B**) CFPAC1 cells treated with shTRIM56 or with TRIM56 knockout (Tr56-KO) were stimulated with rIL-17B, and the cell lysates were immunoblotted with the indicated antibodies. RE indicates the relative expression of the phosphorylated ERK1/2. $N = 3$. (**C**) 293T cells were cotransfected with HA-TRIM56 and Flag-tagged WT or deletion mutant IL-17RB and lysed after treated with rIL-17B for reciprocal co-IP with anti-HA and anti-Flag for immunoblotting. $N = 3$. (**D**) TRIM56-knockdown or TRIM56-knockout CFPAC1 cells were treated with rIL-17B, and the cell lysates were used for coimmunoprecipitation with the indicated antibodies after immunoblotting. $N = 2$. (**E**) IL-17RB–knockout CFPAC1 cells were cotransduced with Flag-tagged WT or mutant IL-17RB and HA-Ub (K63 only) and treated rIL-17B. Cell lysates were immunoprecipitated by HA agarose, followed by immunoblotting with the indicated antibodies. $N = 2$. (**F**) IL-17RB–knockout BxPC3 cells expressing Flag-tagged WT, K333R, K454R, or K470R IL-17RB were treated with rIL-17B, and the cell lysates were coimmunoprecipitated with anti-Flag agarose and immunoblotted with the indicated antibodies. #, heavy chain of immunoglobulin. $N = 2$. (**G**) RNA was isolated from IL-17RB–knockout CFPAC1 cells expressing WT or mutant IL-17RB, and *CCL20* and *TFF1* mRNA expression was measured by RT-qPCR ($n = 6$) after rIL-17B treatment. (**H** and **I**) WT or mutant IL-17RB–expressing cells were also evaluated by a SACF assay ($n = 4$) (H) or an invasion assay ($n = 4$) (I). $N = 2$. Data in (G) to (I) were means ± SD. $^*P < 0.05$ and $^{**}P < 0.01$ by Mann-Whitney test.

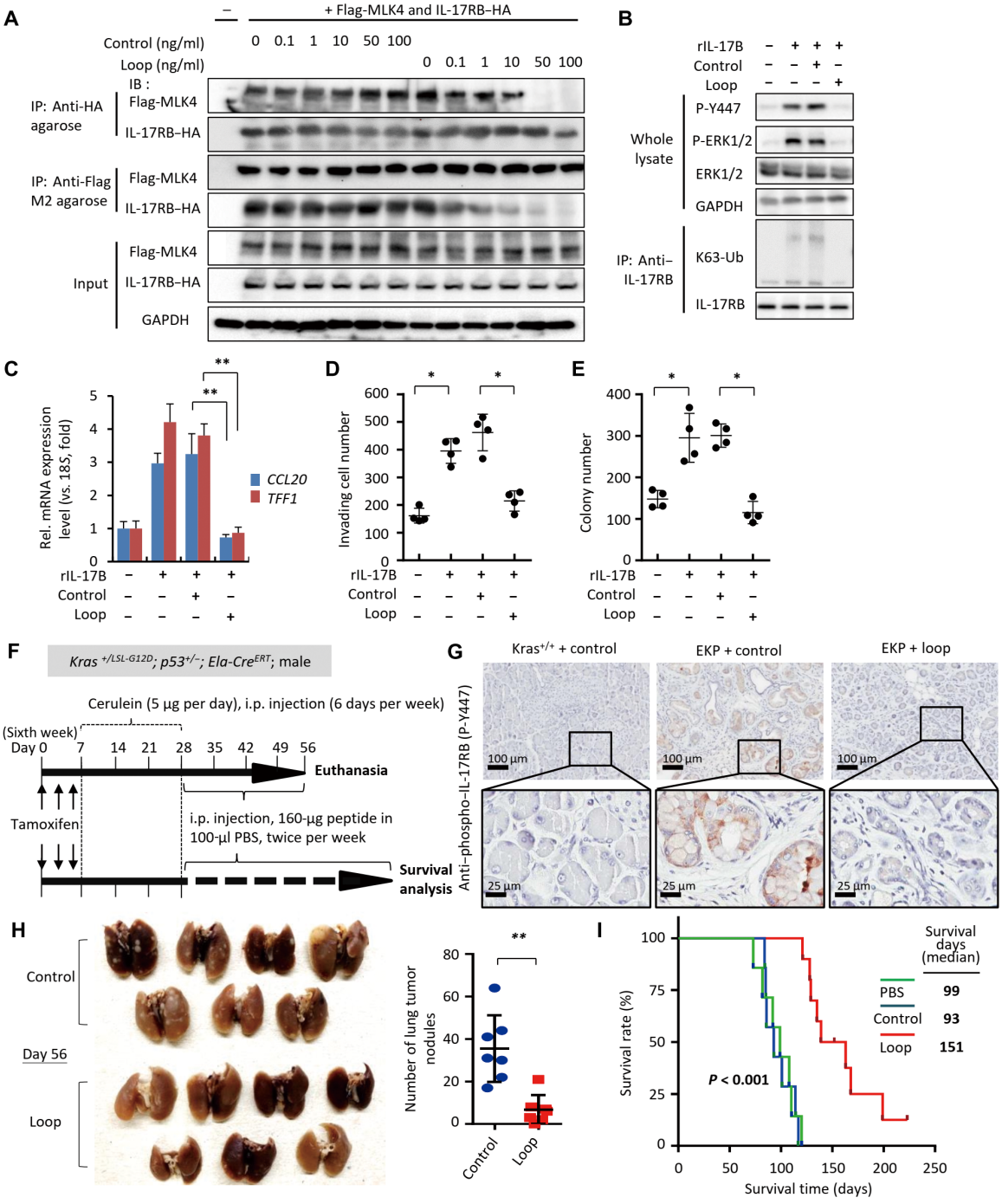

Fig. 7. Disruption of the interaction between IL-17RB and MLK4 by loop peptide treatment blocks oncogenic progression. (**A**) 293T cells expressing Flag-MLK4 and IL-17RB–HA were pretreated with control or loop peptides with indicated dose for 30 min, followed by treatment with rIL-17B for 30 min. The cell lysates were reciprocally coimmunoprecipitated with anti-Flag and anti-HA and blotted with the indicated antibodies. $N = 3$. (**B**) CFPAC1 cells were pretreated with the control or loop peptides for 30 min, followed by treatment with rIL-17B for 30 min. The cell lysates were immunoblotted with the indicated antibodies or immunoprecipitated with anti–IL-17RB or control IgG and blotted with the indicated antibodies. $N = 3$. (**C**) CFPAC1 cells were pretreated with control or loop peptides for 30 min, followed by treatment with rIL-17B for 2 hours. *CCL20* and *TFF1* mRNA expression were measured by RT-qPCR ($n = 6$). (**D** and **E**) CFPAC1 cells treated as in (D) were evaluated by an invasion assay ($n = 4$) (D) and a SACF assay ($n = 4$) (E). $N = 2$. Data in (C) to (E) were means ± SD. *$P < 0.05$ and **$P < 0.01$ by Mann-Whitney test. (**F**) Treatment timeline for pancreatic cancer–bearing transgenic EKP mice (*LSL-Kras*$^{+/G12D}$; *p53*$^{+/–}$; *Ela-Cre*^{ERT}; *plus* cerulein). (**G**) IHC images of EKP mouse pancreases isolated at day 42 after initiation of treatment and stained with anti–P-Y447 antibody. Kras$^{+/+}$ mice (*Kras*$^{+/+}$; *p53*$^{+/–}$; *Ela-Cre*^{ERT}; *plus* cerulein) were used as a control. Boxes indicate enlarged areas. (**H**) Metastatic tumor nodules in the lungs were counted and quantified for EKP mice treated with indicated peptides. **$P < 0.01$ by Mann-Whitney test. (**I**) A Kaplan-Meier curve shows the survival of experimental EKP mice treated with PBS, control peptide, or loop peptide ($n = 7$ for each group). Statistical significance was evaluated using a log-rank test.

phosphorylation of IL-17RB in the pancreatic tissue and quantified lung metastases after euthanizing mice at day 56 after the treatment protocol (Fig. 7F). Treating with the loop peptide, but not the control, diminished the expression of P-Y447 IL-17RB in pancreatic tissues (Fig. 7G), suppressed lung metastasis nodule formation (P = 0.0012; Fig. 7H), and reduced the recruitment of myeloid-derived suppressor cells and M2 macrophages (fig. S15). Similarly, when we measured the survival of mice treated with the loop peptide, loop peptide treatment prolonged life span (P < 0.001; Fig. 7I).

To further explore the therapeutic potential of the loop peptide in human pancreatic cancer cells, we transplanted green fluorescent protein (GFP)– and luciferase-tagged CFPAC1 cells orthotopically into nonobese diabetic–severe combined immunodeficient (NOD-SCID) mice and performed in vivo imaging to monitor pancreatic tumor growth and distant metastasis in livers and lungs using an in vivo imaging system (IVIS) following the protocol, as illustrated (fig. S16A). The control and the loop peptides were injected intraperitoneally into mice bearing pancreatic tumors 7 days after orthotopic implantation of tumor cells. The expression of phosphorylated IL-17RB was inhibited in loop peptide–treated pancreatic tumors (fig. S16B). When we measured tumor burden by IVIS (fig. S16C), we found that treating with the loop peptide significantly impaired tumor growth (P = 0.0012; fig. S16D) and prolonged life span as shown by the Kaplan-Meier survival analysis (P = 0.002; fig. S16E). In a second set of experiments, we euthanized the mice at day 34 after tumor implantation to evaluate the presence of metastases by IVIS imaging. We found that treating with the loop peptide reduced the development of metastases from primary pancreatic tumors to the liver and lung (fig. S16, F and G).

DISCUSSION

IL-17 receptor family members are known for their proinflammatory functions and for promoting an inflammatory microenvironment for tumor progression (*36*). However, unlike other IL-17 receptors, overexpression of IL-17RB confers tumorigenic activity to pancreatic and breast cancers. Mechanistically, IL-17RB forms a homodimer upon IL-17B binding and recruits MLK4 to phosphorylate the Y447 residue of IL-17RB. Phosphorylated IL-17RB, in turn, recruits TRIM56 to add K63-linked ubiquitin chains onto the K470 residue of IL-17RB. Mutation of either Y447 or K470 of IL-17RB abrogated downstream signaling. The biological importance of this signaling mechanism was further demonstrated by blocking MLK4 binding to IL-17RB with a specific peptide containing amino acid sequence 403 to 416 of IL-17RB. Blockade with the loop peptide led to loss of Y477 phosphorylation and K470 ubiquitination, thereby reducing tumorigenesis and metastasis and prolonging the life span of pancreatic tumor–bearing mice (fig. S17).

It is known that IL-17RA serves as the common receptor that forms heterodimer with other IL-17 receptors. IL-17A and IL-17F exist either as homodimers or as a heterodimer, and all forms of the cytokine induce signals through an obligate dimeric IL-17RA and IL-17RC receptor complex (*37*). Similarly, IL-17E (IL-25) induces signals through IL-17RA and IL-17RB heterodimer to amplify T_H2 immune responses (*38*, *39*). Unlike these IL-17 ligands that bind to IL-17RA heterodimers, we found that IL-17B binds to IL-17RB homodimer. A possibility exists that IL-17E may inhibit IL-17RB dimerization and phosphorylation in the context of high IL-17RA expression. This was indeed the case in IL-17RA overexpressing cells as demonstrated. IL-17RB was overexpressed in pancreatic cancer cells (*7*), but the expression of IL-17RA was barely or not detectable, conferring those cells a higher sensitivity to IL-17B than IL-17E response. Moreover, pancreatic cancer cells secreted IL-17B in an autocrine fashion in vitro to facilitate the activation of IL-17RB signaling for promoting cancer progression (*7*). These functional variations and differential distributions of the IL-17 cytokine and receptor family members may contribute to distinct biological functions and disease patterns.

The process of IL-17RB signaling described herein appears to be distinct among the IL-17 receptor family. IL-17B binds to IL-17RB and causes homodimerization, which is required for oncogenic signaling. Unlike RTK receptors, IL-17RB itself is not a kinase and recruits an MLK, MLK4, to phosphorylate Y447 of IL-17RB after homodimerization. This finding highlights the similarity of IL-17RB to an RTK in that both are tyrosine-phosphorylated receptors. It was reported that the tyrosine kinase, Syk, may be involved in IL-17RA signaling (*40*). However, Syk has no influence on IL-17B–induced phosphorylation of IL-17RB and ERK1/2, suggesting that Syk may have little or no role in IL-17RB signaling. Whether other IL-17 heterodimer receptors are phosphorylated by other RTKs in response to their cognate ligands remains to be addressed.

IL-17RB Y447 phosphorylation is required for recruiting TRIM56 E3 ligase to ubiquitinate IL-17RB at residue K470. Although ubiquitination by TRAF6 or ACT1 E3 ligase is observed on other mediators in IL-17RA signaling pathways (*20*, *41*), removal of ACT1 or TRAF6 did not affect IL-17RB K63-linked ubiquitination. The function of K63-linked ubiquitination of IL-17RB is to recruit other factors such as ACT1, which are responsible for transmitting distal signals. ACT1 also relies on its E3 ligase activity for downstream IL-17 signaling transduction, leading to the activation of the nuclear factor κB (NF-κB) and mitogen-activated protein kinase (MAPK) pathways, as well as the C/EBPs pathway (*42*, *43*). Together, these transcription factors drive the transcriptional activation of IL-17 target genes. The IL-17B–induced IL-17RB pathway appears to be involved in the NF-κB and MAPK pathways to activate downstream targeted cytokine genes that promote oncogenesis and metastasis (*6*, *7*).

On the basis of the understanding of these proximal signaling steps, blocking these key steps would likely be effective strategies to inhibit tumor malignancy. Inhibition of IL-17RB activation by neutralizing antibodies has been previously reported (*7*). Similarly, antibody-mediated neutralization of IL-17B is conceivable because blocking IL-17A with antibodies is clinically beneficial to psoriasis (*44*, *45*). However, IL-17RB also serves as the receptor for IL-17E, which promotes T_H2-skewed inflammatory responses critical for immune homeostasis and defense against to bacterial infection (*25*, *26*). Moreover, T_H2 cytokines are linked to tumor growth and metastasis through suppression of the antitumor immunity (*46*, *47*). Therefore, a prolonged therapeutic blockage of IL-17RB signaling such as using anti–IL-17RB antibody might be resulted in deleterious clinical side effects. The finding that TAT–IL-17RB$_{403–416}$ specifically blocks the IL-17RB activation and does not affect T_H2 immune responses, as described herein, provides a better treatment strategy with minimal adverse effects on T_H2 immunity. In addition, we found that the process of TRIM56 ligase mediating IL-17RB K63-linked ubiquitination is essential for IL-17RB oncogenic signaling. On the basis of the above-demonstrated principle, the interaction

surface between TRIM56 and IL-17RB may provide a useful target for blocking this signaling cascade.

However, there are limitations to our study. Using these approaches to pinpointing proximal signal transduction mechanisms does not evaluate conformational changes of the receptor for recruiting other effectors. The current model has to be validated through future cryo–electron microscopy investigation of the IL-17RB receptor complex after stimulation with IL-17B. In addition, further modification of the loop peptide and development of specific small molecules targeting these key steps of the IL-17RB oncogenic signaling are warranted for generating effective drugs. In conclusion, our results explicated that the initial key steps of IL-17RB signaling provide ample opportunities for developing effective peptides or small molecules for treating pancreatic cancer, breast cancer, and other malignancies driven by the IL-17B–mediated IL-17RB downstream signaling pathway (fig. S17).

MATERIALS AND METHODS

Study design

The objective of our study was to elucidate the proximal signaling mechanisms after IL-17B binding to its receptor, IL-17RB, on tumor cells. First, we searched for receptor phosphorylation by immunoblotting analysis with antibodies against modified residues on IL-17RB. A specific antibody against Y447-phosphorylated IL-17RB was made and used to search for the responsible kinase by proteomic analysis. MLK4 was identified as the kinase to phosphorylate IL-17RB and validated its importance by standard oncogenic activity assays. Next, the MLK4-binding site of IL-17RB was mapped by deletion analysis. Further studies demonstrated that the interaction between MLK4 and IL-17RB could be blocked using the described loop peptide, which, in turn, reduced tumor burden in mouse models. Further key step of the downstream signaling pathway was similarly explored, and ubiquitin ligase TRIM56 was identified for adding K63-linked ubiquitin chains to the K470 residue of IL-17RB after phosphorylation of the Y447 residue. All the experiments were repeated at least twice.

All pancreatic cancer patient data and tissue specimens were acquired from the National Taiwan University Hospital (NTUH), Taipei, Taiwan (tables S1 and S2) and approved by the Institutional Review Board of the NTUH (201701015RINA). For independent validation of the P-Y447 IL-17RB as a prognostic marker, tumor specimens isolated from a cohort of 87 patients with pancreatic cancer who underwent surgical resection in NTUH from 2007 to 2015 were used. The pancreatic cancer specimens were collected from patients who underwent pancreatic duodenectomy and had pathologically confirmed pancreatic ductal adenocarcinoma (PDAC). Clinical characteristics of patients in the validation cohort are listed in table S2. The data of the clinical relevance are reported according to REporting recommendations for tumor MARKer prognostic studies (REMARK) guidelines in this paper.

All animal experiments described herein were approved by the Institutional Animal Care and Utilization Committee of Academia Sinica (IACUC no.16-03-945) and China Medical University (IACUC no. 2017-015), Taiwan. Male mice of 8 to 12 weeks old were randomized into groups in an unbiased fashion. The investigators were blinded to group allocation during experiments and outcome assessment. On the basis of pilot experiments, sample sizes were estimated to provide sufficient numbers of mice in each group for statistical analysis.

Cell culture, transfection, and reagent treatment

Human embryonic kidney cell line HEK293T, human pancreatic cancer cell lines AsPC1, BxPC3, CFPAC1, and human breast cancer cell lines MDA-MB-361 and MDA-MB-468 were purchased from the American Type Culture Collection and cultured in a humidified 37°C incubator supplemented with 5% CO_2. These cell lines used in this paper are not listed in the database of misidentified cell lines in National Center for Biotechnology Information BioSample and were not further authenticated after purchase. HEK293T, AsPC1, MDA-MB-361, and MDA-MB-468 cells were maintained in Dulbecco's modified Eagle's medium; BxPC3 cells were cultured in RPMI-1640 medium; and CFPAC1 cells were cultured in Iscove's modified Dulbecco's medium. All media were supplemented with 10% fetal bovine serum, penicillin and streptomycin (100 IU/ml and 100 μg/ml, respectively), and 1× nonessential amino acids. All the media and supplements were purchased from Gibco (Thermo Fisher Scientific). These cell lines were regularly examined for mycoplasma contamination by 4,6-diamidino-2-phenylindole (DAPI) staining and e-Myco Mycoplasma PCR Detection Kit (Bulldog Bio). TransIT-LT1 Transfection Reagent (MIR 2300, Mirus Bio) was used for the transient transfection of plasmids into cells according to the manufacturer's instructions.

Pan-MLK inhibitor CEP-1347 was purchased from Tocris Bioscience. Peptides of $TAT_{48–57}$ (control) and $TAT–IL\text{-}17RB_{403–416}$ (loop peptide) were purchased from TOOLS with a purity of >95%. To assess the effect of IL-17B on IL-17RB signaling, cells were cultured in serum-free medium for 2 hours before adding recombinant IL-17B (rIL-17B; 50 ng/ml) to eliminate endogenous IL-17B interference.

Co-IP assay and immunoblotting analysis

Whole-cell lysates were prepared as previously described (*6*, *7*). Briefly, 500 μg of crude whole-cell extract was incubated with 5 μg of anti–IL-17RB (FGRB, in-house-generated mouse polyclonal) or control normal mouse immunoglobulin G (IgG) (mIgG; 015-000-003, Jackson ImmunoResearch) antibodies at 4°C overnight. Then, 50 μl of prewashed protein A/G agarose beads (sc-2003, Santa Cruz Biotechnology) were added to the mixture and incubated at 4°C for 2 hours with gentle agitation. For reciprocal co-IP, the whole-cell extract was incubated with anti-Flag M2 agarose (A2220, Sigma-Aldrich) or anti-HA (HA-7) agarose (A2095, Sigma-Aldrich) at 4°C for 2 hours with gentle agitation. After extensive washing with diluted lysis buffer (0.01% Triton X-100), IL-17RB and its associated proteins were analyzed by immunoblotting analysis. A Bradford protein assay (Bio-Rad) was used for determining protein concentration.

Immunoblotting analysis was performed after proteins were separated by gradient SDS–polyacrylamide gel electrophoresis (PAGE) (HR gradient gel solution, TFUGG420, TOOLS) and transferred to polyvinylidene difluoride membrane. Samples were incubated overnight with diluted primary antibody, followed by diluted horseradish peroxidase–conjugated anti-rabbit, anti-mouse, or anti-goat antibody (Jackson ImmunoResearch) as described (*48–50*). Mouse monoclonal antibody against IL-17RB (A68; 1:2000) and rabbit anti–P-Y447 polyclonal antibody were generated in house. Other primary antibodies used include antiphosphoserine (P5747; 1:500), anti-Flag (clone M2; 1:2000), and anti-HA (clone HA-7; 1:1000) from Sigma-Aldrich; antiphosphothreonine (clone RM102; 1:500), anti-AAK1 (GTX59663; 1:500), anti-HIPK1 (clone C3; 1:200), and anti–glyceraldehyde-3-phosphate dehydrogenase antibody (GTX627408; 1:10,000) from GeneTex; antiphosphotyrosine (clone PY20; 1:500)

from Merck; anti–p-ERK1/2 (4370; 1:1000) and anti-ERK1/2 (4695; 1:500) from Cell Signaling Technology; anti-MLK4 (ab93798; 1:200) from Abcam; and anti–6-His tag (A109-114; 1:1000) from Bethyl Laboratories. Immunoblot was developed using the Clarity Western ECL Blotting Substrates and ChemiDoc Imaging Systems (Bio-Rad). Optical density was determined using the National Institutes of Health ImageJ program.

Preparation of plasmids, retroviruses, and lentiviruses

Retro-neo control and IL-17RB were cloned into the retroviral vector as previously described (*6*, *7*). The IL-17RB mutants Y338F, Y350F, Y443F, Y447F, Y457F, and Y466F were generated using the QuikChange XL site-directed mutagenesis kit (200516, Agilent) according to the manufacturer's instructions. The wild-type and mutant pQCXIP-IL-17RB plasmids were individually cotransfected with pMD.G (Env-encoding vector) into Gp2-293 cells to generate retroviruses carrying IL-17RB.

Flag-MLK4 and IL-17RB–Flag cloned in pCMV6-Entry were purchased from OriGene. Full-length IL-17RB was subcloned into Eco RI/Eco RV sites of pcDNA3.1 plasmid for expressing C-terminal IL-17RB–HA. IL-17RA–His was constructed by insertion of complementary DNA (cDNA) of IL-17RA at Him DIII site and Bam HI site of pCNA3.1$^+$/myc-His A vector. TRIM56-HA was constructed by insertion of cDNA of TRIM56 at the Him DIII site and Bam HI site of pCNA3.1$^+$/C-HA vector. All the pcDNA3-His-Ubiquitin clones were provided by R.-H. Chen at the Institute of Biological Chemistry, Academia Sinica, Taiwan.

IL-17RB–Flag mutants (FNmut and Y447F), IL-17RB–HA mutants (ΔH346 ~ F354, ΔI373 ~ T384, ΔV403 ~ S416, ΔF423 ~ F430, S423 ~ F430, ΔN458 ~ V462, ΔK470 ~ Q484, and ΔQ484 ~ S502), MLK4 mutants (Δ100-108, E314K, and Y330H), and TRIM56 mutants (Δ31-50) were also generated using the QuikChange XL site-directed mutagenesis kit per the manufacturer's instructions (200516, Agilent).

The lentiviral short hairpin RNA (shRNA) expression vectors of pLKO.1-shLacZ, shMLK4 (mixture of TRCN3212 and TRCN3213), shAAK1 (mixture of TRCN1945 and TRCN1945), shHIPK1 (mixture of TRCN7163 and TRCN7165), TRIM56 (TRCN73094 and TRCN73096), ACT1 (TRCN162747 and TRCN163987), and TRAF6 (TRCN7349, TRCN7350, TRCN7351, and TRCN7352), packaging plasmid pCMVΔR8.91, and pMD.G were obtained from the National RNAi Core Facility of Academia Sinica. For lentivirus production, 293T cells were transfected with 5 μg of pLKO.1-puro lentiviral vectors expressing different shRNAs along with 0.5 μg of envelope plasmid pMD.G and 5 μg of packaging plasmid pCMVΔR8.91 as described (*7*). Viruses were collected 48 hours after transfection. To establish cells depleted with IL-17RB or MLK4, different cell lines including AsPC1, BxPC3, CFPAC1, MDA-MB-361, and MDA-MB-468 were infected with lentiviruses containing the corresponding shRNA for 24 hours and then selected with appropriate antibiotics.

Genome editing of IL-17RB, MLK4, and TRIM56 genes in the pancreatic cancer cell

To introduce DNA double-strand break repair-dependent gene deletion or mutation in IL-17RB, MLK4, and TRIM56 in BxPC3 cells, we used an RNA-guided endonuclease system obtained from the National RNAi Core Facility of Academia Sinica to express the Cas9 endonuclease. The sequences of guide RNA for targeting IL-17RB, MLK4, and TRIM56 are described in table S5. BxPC3 cells were transfected with 10 μg of each plasmid using TransIT-LT1 Transfection Reagent (MIR 2300, Mirus Bio) following the manufacturer's instruction. After 2 days of transfection, we performed a limiting dilution assay to derive single-cell clones and measured the expression of these genes by immunoblotting analysis.

RNA isolation, reverse transcription, and reverse transcription quantitative polymerase chain reaction assays

Total RNA from cultured cells and tumor tissue was isolated using TRIzol reagent (Thermo Fisher Scientific) and reverse-transcribed with the Transcriptor First Strand cDNA Synthesis Kit (Roche Life Science) for gene expression analysis according to the manufacturer's instructions. Reverse transcription quantitative polymerase chain reaction (RT-qPCR) assays were run on the StepOnePlus system (Applied Biosystems) using the KAPA SYBR FAST qPCR Kit (Kapa Biosystems) according to the manufacturer's instructions, and data were analyzed by StepOne software v2.2.2. All the primers were listed in table S5. β-Actin mRNA was used as an internal control. Expression was calculated according to the relative ΔC_t method as described (*7*).

Soft agar colony formation assay and invasion assay

Soft agar colony formation assay was performed as described (*7*). Briefly, 2500 to 10,000 cells were seeded in a layer of 0.35% agar/complete growth medium over a layer of 0.5% agar/complete growth medium in a 12-well plate. Cell medium containing the indicated concentration of rIL-17B (R&D Systems), dimethyl sulfoxide (DMSO) (Sigma-Aldrich), or CEP-1347 (Tocris Bioscience) was replenished every 3 days. On day 14 or 21 after seeding, cells were fixed and stained with pure ethanol containing 0.05% crystal violet (Sigma-Aldrich). Crystal violet–stained colonies greater than 50 μm in size were counted and analyzed objectively by light microscopy.

For invasion assay, about 10^4 cells were seeded in the top chamber with Matrigel-coated membrane (24-well BD Falcon HTS Fluoro Block insert; pore size, 8 μm; BD Biosciences) in serum-free media containing rIL-17B, DMSO, or CEP-1347. Medium supplemented with 10% serum was used as a chemoattractant in the lower chamber. After 24 or 48 hours, the invading cells were fixed with methanol, stained with DAPI, and counted by fluorescence microscopy.

Mass spectrometry

CFPAC1 cells were treated with rIL-17B or bovine serum albumin (50 ng/ml) for 30 min in serum-free conditions after serum starvation for 2 hours. Then, the culture media were removed, and the cells were washed with phosphate-buffered saline (PBS). Crosslinker dithiobis(succinimidyl propionate) (Thermo Fisher Scientific) dissolved in PBS was used to treat the cells for 30 min, and the reaction was stopped by adding tris buffer (50 mM) (pH 8.0). Whole cell lysate was collected and incubated with anti–IL-17RB antibody for co-IP. The IL-17RB–interacting proteins were separated by SDS-PAGE, and the protein bands from SDS-PAGE were subjected to in-gel trypsin/chymotrypsin digestion after standard procedure and then analyzed by MS. The procedures and data analysis were performed as described (*48*) and done in Academia Sinica Common Mass Spectrometry facilities. Briefly, the enzyme-digested protein samples were injected onto a self-packed precolumn (150 μm of inside diameter × 20 mm, 5 μm, 200 Å). Chromatographic separation was performed on self-packed reversed-phase C18 nanocolumn (75 μm of inside diameter × 300 mm, 5 μm, 100 Å) using 0.1% formic

acid in water (mobile phase A) and 0.1% formic acid in 80% acetonitrile (mobile phase B). A linear gradient was applied from 5 to 45% mobile phase B for 40 min at a flow rate of 300 nl/min. Electrospray voltage was applied at 2 kV, and capillary temperature was set at 200°C. A scan cycle was initiated with a full-scan survey MS spectrum [mass/charge ratio (m/z), 300 to 2000] performed on a Fourier Transform Ion Cyclotron Resonance (FT-ICR) mass spectrometer with a resolution of 100,000 at 400 Da. The 10 most abundant ions detected in this scan were subjected to a tandem MS experiment performed with an Linear Trap Quadropole (LTQ) mass spectrometer. Ion accumulation (auto gain control target number) and maximum ion accumulation time for the full scan and tandem MS were set at 1×10^6 ions, 1000 ms, and 5×10^4 ions, 200 ms, respectively. Ions were fragmented by use of collision-induced dissociation with the normalized collision energy set to 35%, activation Q set to 0.3, and an activation time of 30 ms.

Analysis of IL-17 receptor oligomerization by immunoprecipitation

BxPC3 IL-17RB–knockout cells were transiently cotransfected with IL-17RB–HA, IL-17RB–Flag, and IL-17RA–His plasmids using TransIT-LT1 Transfection Reagent (MIR 2300, Mirus Bio) according to the manufacturer's instructions. The cells were then treated with indicated concentrations of rIL-17B or rIL-17E for the indicated times and lysed for co-IP assay using different antibodies as described above.

DuoLink in situ interaction assay

DuoLink PLA Kit (DuoLink, DUO92101, Sigma-Aldrich) was used to detect protein-protein interaction using fluorescence microscopy as in the manufacturer's protocol. Briefly, pancreatic cancer cells were treated with rIL-17B at the indicated concentration for 30 min in eight-chamber microscope slides after serum starvation for 2 hours, fixed with 4% paraformaldehyde for 15 min at room temperature, permeabilized with 0.2% Triton X-100, and blocked with DuoLink blocking buffer for 30 min at 37°C. The cells were then incubated with primary antibodies diluted in DuoLink antibody diluents for 1 hour. The primary antibodies sets used differed for each distinct experiment: Antibodies against IL-17RB (FGRB, homemade) and MLK4 (rabbit, ab93798, Abcam) were used in Fig. 3F, antibodies against Flag tag (mouse, F7425, Sigma-Aldrich) and HA tag (rabbit, HA-7, Sigma-Aldrich) were used in Fig. 4C and fig. S6D, and antibodies against IL-17RB (D9) native form was used in Fig. 4D. After that, the cells were washed and further incubated for 1 hour at 37°C with species-specific secondary antibody carrying PLA probes for hybridization, which was facilitated by close proximity of less than 16 nm in the presence of two complementary oligonucleotides. After annealing and rolling circle amplification, a detection solution consisting of fluorescently labeled oligonucleotides was added, and the slides were mounted with Fluoroshield with DAPI (GeneTex). The signal was detected as distinct fluorescent dots in the Texas red channel. Microscopy images were acquired by confocal spectral microscopy (Leica SP2/SP8X) and analyzed by LAS AF software (Leica Biosystems). Negative controls consisted of samples treated as described above but with secondary antibodies alone.

Immunohistochemistry

Formalin-fixed paraffin-embedded primary tumor tissue sections were used for IHC. Heat-induced antigen retrieval was performed using 0.1 M citrate buffer (pH 6.0) and autoclaving for 20 min. Endogenous peroxidase was eliminated with 3% H_2O_2. Slides were stained with an in-house–generated anti–IL-17RB antibody (A81; 1:2000) and anti–P-Y447 (1:500), respectively, in PBS with 10% fetal bovine serum overnight at 4°C. After washing, slides were incubated with anti-rabbit/mouse horseradish peroxidase polymer before visualization with liquid diaminobenzidine tetrahydrochloride and substrate diaminobenzidine chromogen from Dako REAL EnVision. All slides were counterstained with hematoxylin.

In vivo tumor models

For the spontaneous pancreatic cancer model, $Kras^+$/LSLG12D mice (B6;129-Kras2) bearing the Cre-dependent conditional knockin mutation KrasG12D were obtained from the Mouse Models of Human Cancer Consortium (*51*). $Kras^+$/LSLG12D mice were bred with Elas-CreER mice obtained from the Level Transgenic Center (*33*–*35*, *52*) to generate Elas-$CreER^T$;$Kras^+$/LSLG12D mice. To induce the expression of $Kras^+$/LSLG12D in acinar cells, 5-week-old Elas-$CreER^T$;$Kras^+$/LSLG12D male mice were intraperitoneally injected with 100 μl of free base tamoxifen (20 mg/ml in corn oil; Sigma-Aldrich) three times per week (three injections of 2 mg each) for 1 week. Those mice were then intraperitoneally injected with 100 μl of cerulein (50 μg/ml) (BACHEM) in PBS six times per week (six injections of 5 μg each) for 3 weeks to induce chronic inflammation and tumors. The animals were intraperitoneally injected with PBS, control ($TAT_{49–57}$) peptide, or loop (TAT–IL-$17RB_{403–416}$) peptide, and tumor burden was monitored.

For the orthotopic pancreatic cancer model, human pancreatic tumor cells expressing GFP and luciferase were injected into 6-week-old NOD-SCID female mice. These mice were first anesthetized using continuous isoflurane (3.5%), and their abdomen was sterilized. We then performed a laparotomy (5 to 10 mm) over the left upper quadrant of the abdomen to expose the peritoneal cavity. The pancreas was exteriorized onto a sterile field, and sterile PBS or 5×10^5 pancreatic tumor CFPAC1 cells suspended in 25 μl of sterile PBS were injected into the tail of the pancreas via a 30-gauge needle (Covidien). Successful injection was confirmed by the formation of a liquid bleb at the site of injection with minimal fluid leakage. The pancreas was then gently placed back into the peritoneal cavity. The peritoneum was then closed with a 5-0 PDS II violet suture (Ethicon), and the skin was closed using the AutoClip system (Braintree Scientific). In vivo bioluminescence signal was assessed as a surrogate for tumor burden and analyzed with the IVIS Spectrum In Vivo Imaging System (PerkinElmer).

Statistical analysis

We chose our sample sizes based on those commonly used in this field without predetermination by statistical methods. Except for the clinical correlation and quantification for specific immunoblots, all data were presented as means ± SD, and two-tailed Mann-Whitney test was used to compare control and treatment groups. Asterisks (*) and (**) indicate statistical significance with $P < 0.05$ and $P < 0.01$, respectively. The following analyses were performed using GraphPad Prism 6 and SPSS statistics software. The Kaplan-Meier estimation method was used for the overall survival analysis of the tumor-bearing mice, and a log-rank test was used to compare the differences between groups.

SUPPLEMENTARY MATERIALS

stm.sciencemag.org/cgi/content/full/13/583/eabc2823/DC1

Materials and Methods

Fig. S1. Knockout of IL-17RB diminishes IL-17B signaling.

Fig. S2. Mutation of tyrosine-447 of IL-17RB abrogates IL-17B–induced signaling.

Fig. S3. IHC images of primary and metastatic pancreatic tumor specimens using anti–P-Y447 antibody.
Fig. S4. Depletion of AAK1, HIPK1, or Syk does not alter IL-17B–induced ERK1/2 phosphorylation.
Fig. S5. Knockdown of MLK4 expression reduces IL-17B–induced ERK1/2 phosphorylation, CCL20 and TFF1 expression, and invasion ability of pancreatic and breast cancer cells.
Fig. S6. IL-17B, but not IL-17E, induces IL-17RB tyrosine phosphorylation, and FNmut IL-17RB fails to homodimerize.
Fig. S7. Overexpression of IL-17RA or treating with IL-17E reduces IL-17B–mediated IL-17RB dimerization and tyrosine phosphorylation.
Fig. S8. IL-17B–induced IL-17RB dimerization was not affected by knockdown of TRIM56, MLK4, or mutations of Y447 and K470 of IL-17RB.
Fig. S9. CEP-1347 inhibits IL-17RB Y447 phosphorylation, ERK1/2 phosphorylation, and invasiveness of both pancreatic and breast cancer cells.
Fig. S10. Predicted structure of the SEFIR domain of human IL-17RB and the steric conformation of Y447.
Fig. S11. TRIM56 binds to N458-V462 of IL-17RB and is critical for IL-17RB signaling in vitro.
Fig. S12. TRIM56 serves as an E3 ligase for K63-linked ubiquitination of IL-17RB.
Fig. S13. Treatment with loop peptide suppresses invasiveness and colony forming in pancreatic tumor cells in vitro.
Fig. S14. Loop peptide does not suppress IL-17E–induced IL-4 and IL-13 mRNA expression in peripheral blood mononuclear cells or affect bone marrow–derived dendritic cell activation.
Fig. S15. Treatment with loop peptide reduces the recruitment of myeloid-derived suppressor cells and M2 macrophages.
Fig. S16. Disruption of the IL-17RB and MLK4 interaction by loop peptide treatment suppresses pancreatic tumor progression.
Fig. S17. Graphical summary.
Table S1. Univariate and multivariate Cox regression analysis of the influence of IL-17RB phosphorylation on overall survival.
Table S2. Phosphorylation of residue Y447 of IL-17RB in pancreatic tumor specimens correlates with worse clinical progression.
Table S3. List of proteins interacting with IL-17RB after IL-17B treatment.
Table S4. List of proteins coimmunoprecipitated with wild-type IL-17RB, but not Y447F-mutant IL-17RB, after IL-17B treatment.
Table S5. List of the primers used in this paper.
Data file S1. Individual-level data.

View/request a protocol for this paper from *Bio-protocol*.

REFERENCES AND NOTES

1. Y. Iwakura, H. Ishigame, S. Saijo, S. Nakae, Functional specialization of interleukin-17 family members. *Immunity* **34**, 149–162 (2011).
2. S. Aggarwal, A. L. Gurney, IL-17: Prototype member of an emerging cytokine family. *J. Leukoc. Biol.* **71**, 1–8 (2002).
3. M. Novatchkova, A. Leibbrandt, J. Werzowa, A. Neubuser, F. Eisenhaber, The STIR-domain superfamily in signal transduction, development and immunity. *Trends Biochem. Sci.* **28**, 226–229 (2003).
4. V. Ramirez-Carrozzi, A. Sambandam, E. Luis, Z. Lin, S. Jeet, J. Lesch, J. Hackney, J. Kim, M. Zhou, J. Lai, Z. Modrusan, T. Sai, W. Lee, M. Xu, P. Caplazi, L. Diehl, J. de Voss, M. Balazs, L. Gonzalez Jr., H. Singh, W. Ouyang, R. Pappu, IL-17C regulates the innate immune function of epithelial cells in an autocrine manner. *Nat. Immunol.* **12**, 1159–1166 (2011).
5. Y. Su, J. Huang, X. Zhao, H. Lu, W. Wang, X. O. Yang, Y. Shi, X. Wang, Y. Lai, C. Dong, Interleukin-17 receptor D constitutes an alternative receptor for interleukin-17A important in psoriasis-like skin inflammation. *Sci. Immunol.* **4**, eaau9657 (2019).
6. C. K. Huang, C. Y. Yang, Y. M. Jeng, C. L. Chen, H. H. Wu, Y. C. Chang, C. Ma, W. H. Kuo, K. J. Chang, J. Y. Shew, W. H. Lee, Autocrine/paracrine mechanism of interleukin-17B receptor promotes breast tumorigenesis through NF-κB-mediated antiapoptotic pathway. *Oncogene* **33**, 2968–2977 (2014).
7. H.-H. Wu, W. W. Hwang-Verslues, W.-H. Lee, C.-K. Huang, P.-C. Wei, C.-L. Chen, J.-Y. Shew, E. Y.-H. P. Lee, Y.-M. Jeng, Y.-W. Tien, C. Ma, W.-H. Lee, Targeting IL-17B–IL-17RB signaling with an anti–IL-17RB antibody blocks pancreatic cancer metastasis by silencing multiple chemokines. *J. Exp. Med.* **212**, 333–349 (2015).
8. A. Maitra, F. Shen, W. Hanel, K. Mossman, J. Tocker, D. Swart, S. L. Gaffen, Distinct functional motifs within the IL-17 receptor regulate signal transduction and target gene expression. *Proc. Natl. Acad. Sci. U.S.A.* **104**, 7506–7511 (2007).
9. R. M. Onishi, S. J. Park, W. Hanel, A. W. Ho, A. Maitra, S. L. Gaffen, SEF/IL-17R (SEFIR) is not enough: An extended SEFIR domain is required for il-17RA-mediated signal transduction. *J. Biol. Chem.* **285**, 32751–32759 (2010).
10. B. Zhang, C. Liu, W. Qian, Y. Han, X. Li, J. Deng, Structure of the unique SEFIR domain from human interleukin 17 receptor A reveals a composite ligand-binding site containing a conserved α-helix for Act1 binding and IL-17 signaling. *Acta Crystallogr. D Biol. Crystallogr.* **70**, 1476–1483 (2014).
11. A. V. Garg, M. Ahmed, A. N. Vallejo, A. Ma, S. L. Gaffen, The deubiquitinase A20 mediates feedback inhibition of interleukin-17 receptor signaling. *Sci. Signal.* **6**, ra44 (2013).
12. A. V. Garg, S. L. Gaffen, IL-17 signaling and A20: A balancing act. *Cell Cycle* **12**, 3459–3460 (2013).
13. S. Zhu, W. Pan, P. Shi, H. Gao, F. Zhao, X. Song, Y. Liu, L. Zhao, X. Li, Y. Shi, Y. Qian, Modulation of experimental autoimmune encephalomyelitis through TRAF3-mediated suppression of interleukin 17 receptor signaling. *J. Exp. Med.* **207**, 2647–2662 (2010).
14. B. Zhang, C. Liu, W. Qian, Y. Han, X. Li, J. Deng, Crystal structure of IL-17 receptor B SEFIR domain. *J. Immunol.* **190**, 2320–2326 (2013).
15. F. McAllister, J. M. Bailey, J. Alsina, C. J. Nirschl, R. Sharma, H. Fan, Y. Rattigan, J. C. Roeser, R. H. Lankapalli, H. Zhang, E. M. Jaffee, C. G. Drake, F. Housseau, A. Maitra, J. K. Kolls, C. L. Sears, D. M. Pardoll, S. D. Leach, Oncogenic Kras activates a hematopoietic-to-epithelial IL-17 signaling axis in preinvasive pancreatic neoplasia. *Cancer Cell* **25**, 621–637 (2014).
16. S. Furuta, Y.-M. Jeng, L. Zhou, L. Huang, I. Kuhn, M. J. Bissell, W.-H. Lee, IL-25 causes apoptosis of IL-25R–expressing breast cancer cells without toxicity to nonmalignant cells. *Sci. Transl. Med.* **3**, 78ra31 (2011).
17. S.-C. Huang, P.-C. Wei, W. W. Hwang-Verslues, W.-H. Kuo, Y.-M. Jeng, C.-M. Hu, J.-Y. Shew, C.-S. Huang, K.-J. Chang, E. Y.-H. P. Lee, W.-H. Lee, TGF-β1 secreted by Tregs in lymph nodes promotes breast cancer malignancy via up-regulation of IL-17RB. *EMBO Mol. Med.* **9**, 1660–1680 (2017).
18. S. R. Hubbard, W. T. Miller, Receptor tyrosine kinases: Mechanisms of activation and signaling. *Curr. Opin. Cell Biol.* **19**, 117–123 (2007).
19. S. M. Craige, M. M. Reif, S. Kant, Mixed - Lineage Protein kinases (MLKs) in inflammation, metabolism, and other disease states. *Biochim. Biophys. Acta* **1862**, 1581–1586 (2016).
20. S. L. Gaffen, Structure and signalling in the IL-17 receptor family. *Nat. Rev. Immunol.* **9**, 556–567 (2009).
21. J. M. Kramer, L. Yi, F. Shen, A. Maitra, X. Jiao, T. Jin, S. L. Gaffen, Cutting Edge: Evidence for ligand-independent multimerization of the IL-17 receptor. *J. Immunol.* **176**, 711–715 (2006).
22. J. M. Kramer, W. Hanel, F. Shen, N. Isik, J. P. Malone, A. Maitra, W. Sigurdson, D. Swart, J. Tocker, T. Jin, S. L. Gaffen, Cutting edge: Identification of a pre-ligand assembly domain (PLAD) and ligand binding site in the IL-17 receptor. *J. Immunol.* **179**, 6379–6383 (2007).
23. Y. Shi, S. J. Ullrich, J. Zhang, K. Connolly, K. J. Grzegorzewski, M. C. Barber, W. Wang, K. Wathen, V. Hodge, C. L. Fisher, H. Olsen, S. M. Ruben, I. Knyazev, Y. H. Cho, V. Kao, K. A. Wilkinson, J. A. Carrell, R. Ebner, A novel cytokine receptor-ligand pair: Identification, molecular characterization, and in vivo immunomodulatory activity. *J. Biol. Chem.* **275**, 19167–19176 (2000).
24. E. Tian, J. R. Sawyer, D. A. Largaespada, N. A. Jenkins, N. G. Copeland, J. D. Shaughnessy Jr., ***Evi27*** encodes a novel membrane protein with homology to the IL17 receptor. *Oncogene* **19**, 2098–2109 (2000).
25. V. Dolgachev, B. C. Petersen, A. L. Budelsky, A. A. Berlin, N. W. Lukacs, Pulmonary IL-17E (IL-25) production and IL-17RB$^+$ myeloid cell-derived Th2 cytokine production are dependent upon stem cell factor-induced responses during chronic allergic pulmonary disease. *J. Immunol.* **183**, 5705–5715 (2009).
26. E. A. Rickel, L. A. Siegel, B.-R. Yoon, J. B. Rottman, D. G. Kugler, D. A. Swart, P. M. Anders, J. E. Tocker, M. R. Comeau, A. L. Budelsky, Identification of functional roles for both IL-17RB and IL-17RA in mediating IL-25-induced activities. *J. Immunol.* **181**, 4299–4310 (2008).
27. A. Rana, B. Rana, R. Mishra, G. Sondarva, V. Rangasamy, S. Das, N. Viswakarma, A. Kanthasamy, Mixed lineage kinase–c-Jun N-terminal kinase axis: A potential therapeutic target in cancer. *Genes Cancer* **4**, 334–341 (2013).
28. M. Martini, M. Russo, S. Lamba, E. Vitiello, E. H. Crowley, F. Sassi, D. Romanelli, M. Frattini, A. Marchetti, A. Bardelli, Mixed lineage kinase MLK4 is activated in colorectal cancers where it synergistically cooperates with activated RAS signaling in driving tumorigenesis. *Cancer Res.* **73**, 1912–1921 (2013).
29. A. Rana, K. Gallo, P. Godowski, S. Hirai, S. Ohno, L. Zon, J. M. Kyriakis, J. Avruch, The mixed lineage kinase SPRK phosphorylates and activates the stress-activated protein kinase activator, SEK-1. *J. Biol. Chem.* **271**, 19025–19028 (1996).
30. A. A. Marusiak, N. L. Stephenson, H. Baik, E. W. Trotter, Y. Li, K. Blyth, S. Mason, P. Chapman, L. A. Puto, J. A. Read, C. Brassington, H. K. Pollard, C. Phillips, I. Green, R. Overman, M. Collier, E. Testoni, C. J. Miller, T. Hunter, O. J. Sansom, J. Brognard, Recurrent MLK4 loss-of-function mutations suppress JNK signaling to promote colon tumorigenesis. *Cancer Res.* **76**, 724–735 (2016).
31. T. Tsuchida, J. Zou, T. Saitoh, H. Kumar, T. Abe, Y. Matsuura, T. Kawai, S. Akira, The ubiquitin ligase TRIM56 regulates innate immune responses to intracellular double-stranded DNA. *Immunity* **33**, 765–776 (2010).
32. Y. Qian, C. Liu, J. Hartupee, C. Z. Altuntas, M. F. Gulen, D. Jane-Wit, J. Xiao, Y. Lu, N. Giltiay, J. Liu, T. Kordula, Q.-W. Zhang, B. Vallance, S. Swaidani, M. Aronica, V. K. Tuohy, T. Hamilton, X. Li, The adaptor Act1 is required for interleukin 17-dependent signaling associated with autoimmune and inflammatory disease. *Nat. Immunol.* **8**, 247–256 (2007).

33. C.-C. Hsieh, Y.-M. Shyr, W.-Y. Liao, T.-H. Chen, S.-E. Wang, P.-C. Lu, P.-Y. Lin, Y.-B. Chen, W.-Y. Mao, H.-Y. Han, M. Hsiao, W.-B. Yang, W.-S. Li, Y.-P. Sher, C.-N. Shen, Elevation of β-galactoside α2,6-sialyltransferase 1 in a fructoseresponsive manner promotes pancreatic cancer metastasis. *Oncotarget* **8**, 7691–7709 (2017).
34. S. C. Tang, L. Baeyens, C. N. Shen, S. J. Peng, H. J. Chien, D. W. Scheel, C. E. Chamberlain, M. S. German, Human pancreatic neuro-insular network in health and fatty infiltration. *Diabetologia* **61**, 168–181 (2018).
35. S. C. Tang, C. N. Shen, P. Y. Lin, S. J. Peng, H. J. Chien, Y. H. Chou, C. E. Chamberlain, P. J. Pasricha, Pancreatic neuro-insular network in young mice revealed by 3D panoramic histology. *Diabetologia* **61**, 158–167 (2018).
36. G. Murugaiyan, B. Saha, Protumor vs antitumor functions of IL-17. *J. Immunol.* **183**, 4169–4175 (2009).
37. N. Amatya, A. V. Garg, S. L. Gaffen, IL-17 signaling: The Yin and the Yang. *Trends Immunol.* **38**, 310–322 (2017).
38. P. G. Fallon, S. J. Ballantyne, N. E. Mangan, J. L. Barlow, A. Dasvarma, D. R. Hewett, A. McIlgorm, H. E. Jolin, A. N. J. McKenzie, Identification of an interleukin (IL)-25–dependent cell population that provides IL-4, IL-5, and IL-13 at the onset of helminth expulsion. *J. Exp. Med.* **203**, 1105–1116 (2006).
39. A. M. Owyang, C. Zaph, E. H. Wilson, K. J. Guild, T. McClanahan, H. R. P. Miller, D. J. Cua, M. Goldschmidt, C. A. Hunter, R. A. Kastelein, D. Artis, Interleukin 25 regulates type 2 cytokine-dependent immunity and limits chronic inflammation in the gastrointestinal tract. *J. Exp. Med.* **203**, 843–849 (2006).
40. N.-L. Wu, D.-Y. Huang, H.-N. Tsou, Y.-C. Lin, W.-W. Lin, Syk mediates IL-17-induced CCL20 expression by targeting Act1-dependent K63-linked ubiquitination of TRAF6. *J. Invest. Dermatol.* **135**, 490–498 (2015).
41. Z. Rong, L. Cheng, Y. Ren, Z. Li, Y. Li, X. Li, H. Li, X.-Y. Fu, Z. Chang, Interleukin-17F signaling requires ubiquitination of interleukin-17 receptor via TRAF6. *Cell. Signal.* **19**, 1514–1520 (2007).
42. M. J. Ruddy, G. C. Wong, X. K. Liu, H. Yamamoto, S. Kasayama, K. L. Kirkwood, S. L. Gaffen, Functional cooperation between interleukin-17 and tumor necrosis factor-α is mediated by CCAAT/enhancer-binding protein family members. *J. Biol. Chem.* **279**, 2559–2567 (2004).
43. Z. Yao, S. L. Painter, W. C. Fanslow, D. Ulrich, B. M. Macduff, M. K. Spriggs, R. J. Armitage, Human IL-17: A novel cytokine derived from T cells. *J. Immunol.* **155**, 5483–5486 (1995).
44. C. E. M. Griffiths, K. Reich, M. Lebwohl, P. van de Kerkhof, C. Paul, A. Menter, G. S. Cameron, J. Erickson, L. Zhang, R. J. Secrest, S. Ball, D. K. Braun, O. O. Osuntokun, M. P. Heffernan, B. J. Nickoloff, K. Papp; UNCOVER-2 and UNCOVER-3 investigators, Comparison of ixekizumab with etanercept or placebo in moderate-to-severe psoriasis (UNCOVER-2 and UNCOVER-3): Results from two phase 3 randomised trials. *Lancet* **386**, 541–551 (2015).
45. P. J. Mease, I. B. McInnes, B. Kirkham, A. Kavanaugh, P. Rahman, D. van der Heijde, R. Landewé, P. Nash, L. Pricop, J. Yuan, H. B. Richards, S. Mpofu; FUTURE Study Group, Secukinumab inhibition of interleukin-17A in patients with psoriatic arthritis. *N. Engl. J. Med.* **373**, 1329–1339 (2015).
46. A. Budhu, M. Forgues, Q.-H. Ye, H.-L. Jia, P. He, K. A. Zanetti, U. S. Kammula, Y. Chen, L.-X. Qin, Z.-Y. Tang, X. W. Wang, Prediction of venous metastases, recurrence, and prognosis in hepatocellular carcinoma based on a unique immune response signature of the liver microenvironment. *Cancer Cell* **10**, 99–111 (2006).
47. R. F. Gabitass, N. E. Annels, D. D. Stocken, H. A. Pandha, G. W. Middleton, Elevated myeloid-derived suppressor cells in pancreatic, esophageal and gastric cancer are an independent prognostic factor and are associated with significant elevation of the Th2 cytokine interleukin-13. *Cancer Immunol. Immunother.* **60**, 1419–1430 (2011).
48. C.-M. Hu, S.-C. Tien, P.-K. Hsieh, Y.-M. Jeng, M.-C. Chang, Y.-T. Chang, Y.-J. Chen, Y.-J. Chen, E. Y.-H. P. Lee, W.-H. Lee, High glucose triggers nucleotide imbalance through O-GlcNAcylation of key enzymes and induces KRAS mutation in pancreatic cells. *Cell Metab.* **29**, 1334–1349.e10 (2019).
49. C.-K. Huang, P.-H. Chang, W.-H. Kuo, C.-L. Chen, Y.-M. Jeng, K.-J. Chang, J.-Y. Shew, C.-M. Hu, W.-H. Lee, Adipocytes promote malignant growth of breast tumours with monocarboxylate transporter 2 expression via β-hydroxybutyrate. *Nat. Commun.* **8**, 14706 (2017).
50. P.-C. Wei, Y.-H. Hsieh, M.-I. Su, X. Jiang, P.-H. Hsu, W.-T. Lo, J.-Y. Weng, Y.-M. Jeng, J.-M. Wang, P.-I. Chen, Y.-C. Chang, K.-F. Lee, M.-D. Tsai, J.-Y. Shew, W.-H. Lee, Loss of the oxidative stress sensor NPGPx compromises GRP78 chaperone activity and induces systemic disease. *Mol. Cell* **48**, 747–759 (2012).
51. E. L. Jackson, N. Willis, K. Mercer, R. T. Bronson, D. Crowley, R. Montoya, T. Jacks, D. A. Tuveson, Analysis of lung tumor initiation and progression using conditional expression of oncogenic *K-ras*. *Genes Dev.* **15**, 3243–3248 (2001).
52. S.-Y. Wu, C.-C. Hsieh, R.-R. Wu, J. Susanto, T.-T. Liu, C.-R. Shen, Y. Chen, C.-C. Su, F.-P. Chang, H.-M. Chang, D. Tosh, C.-N. Shen, Differentiation of pancreatic acinar cells to hepatocytes requires an intermediate cell type. *Gastroenterology* **138**, 2519–2530 (2010).

Acknowledgments: We thank A. Ball for critical reading and suggestions; the RNAi core of the Genomics Research Center, Academia Sinica, Taiwan, for providing shRNA plasmids; and Mouse Models of Human Cancer Consortium (NCI-MMHCC) for providing $Kras^{+}/LSL^{G12D}$ ($LSL\text{-}Kras^{G12D}$) mice. **Funding:** This work was supported and funded by the summit project (AS-SUMMIT-109 to W.-H.L.) and thematic project (AS-107-TP-L15-2 to W.-H.L.) of Academia Sinica, Taiwan; the higher education sprout project by the Ministry of Education (MOE), Taiwan via the "Drug Development Center of China Medical University," CMUH grant (MOHW107-TDU-B-212-114024 to W.-H.L.), and CMU grant (CMU107-TU-10 to H.-H.W.); and Ministry of Science and Technology (MOST) grants (MOST2320-B-039, -052-MY3, MOST 0210-01-13, AS-KPQ-109-BioMed, and MOST 0210-01-18 to W.-H.L. and H.-H.W.). **Author contributions:** Conception and design: H.-H.W. and W.-H.L. Acquisition of data (provided animals, acquired and managed patients, and provided facilities): H.-H.W., C.-M.H., E.Y.-H.P.L., M.-C.C., Y.-T.C., Y.-W.T., Y.-M.J., and W.-H.L. Analysis and interpretation of data, including statistical analysis, biostatistics, and computational analysis: H.-H.W., L.-H.T., P.-H.H., C.-N.S., C.-K.H., M.-Y.C., Y.-I.C., and C.-C.L. Writing, review, and revision of the manuscript: H.-H.W., C.-M.H., C.-K.H., and W.-H.L. Study supervision: H.-H.W. and W.-H.L. **Competing interests:** A patent application titled "Antagonist of interleukin-17B receptor (IL-17RB) and use thereof" (application no. 63/125,148) has been filed, and W.-H.L., H.-H.W., C.-M.H., and C.-K.H. are coinventors. **Data and materials availability:** All data associated with this study are present in the paper or the Supplementary Materials. The full MS data have been deposited to the Proteome Xchange Consortium via the PRIDE partner repository with the dataset identifiers PXD013802. All materials, including chemical compounds as supplies, are available through a standard material transfer agreement to W.-H.L. and H.-H.W.

Submitted 17 April 2020
Resubmitted 7 September 2020
Accepted 21 January 2021
Published 3 March 2021
10.1126/scitranslmed.abc2823

Citation: H.-H. Wu, L.-H. Tsai, C.-K. Huang, P.-H. Hsu, M.-Y. Chen, Y.-I. Chen, C.-M. Hu, C.-N. Shen, C.-C. Lee, M.-C. Chang, Y.-T. Chang, Y.-W. Tien, Y.-M. Jeng, E. Y.-H. Lee, W.-H. Lee, Characterization of initial key steps of IL-17 receptor B oncogenic signaling for targeted therapy of pancreatic cancer. *Sci. Transl. Med.* **13**, eabc2823 (2021).